INTEGRATED OPTICAL CIRCUIT COMPONENTS

NAVAL ELECTRONICS LABORATORY CENTER

PREPARED FOR
ADVANCED RESEARCH PROJECTS AGENCY

17 SEPTEMBER 1974

UNCLASSIFIED

SECURITY CLASSIFICATION OF THIS PAGE (When Data Entered)

REPORT DOCUMENTATION PAGE		READ INSTRUCTIONS BEFORE COMPLETING FORM
1. REPORT NUMBER NELC Technical Report 1931 (TR 1931)	2. GOVT ACCESSION NO.	3. RECIPIENT'S CATALOG NUMBER AD/A-002459
4. TITLE (and Subtitle) INTEGRATED OPTICAL CIRCUIT COMPONENTS (Presents the utilization of integrated optical circuits and fiber optics in Navy and other DoD communications systems)		5. TYPE OF REPORT & PERIOD COVERED Research and Development 1 October to 30 December 1973 6. PERFORMING ORG. REPORT NUMBER
7. AUTHOR(s) W. M. Caton		8. CONTRACT OR GRANT NUMBER(s)
9. PERFORMING ORGANIZATION NAME AND ADDRESS Naval Electronics Laboratory Center San Diego, California 92152		10. PROGRAM ELEMENT, PROJECT, TASK AREA & WORK UNIT NUMBERS ARPA Order 2158, Amendment 1, Program Code 3010, F215.01, Element 61101E (NELC F215)
11. CONTROLLING OFFICE NAME AND ADDRESS Advanced Research Projects Agency		12. REPORT DATE 17 September 1974 13. NUMBER OF PAGES 66
14. MONITORING AGENCY NAME & ADDRESS(if different from Controlling Office)		15. SECURITY CLASS. (of this report) Unclassified 15a. DECLASSIFICATION/DOWNGRADING SCHEDULE

16. DISTRIBUTION STATEMENT (of this Report)

Approved for public release; distribution is unlimited

17. DISTRIBUTION STATEMENT (of the abstract entered in Block 20, if different from Report)

PRICES SUBJECT TO CHANGE

18. SUPPLEMENTARY NOTES

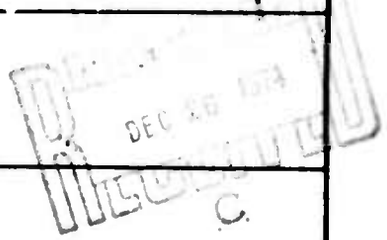

19. KEY WORDS (Continue on reverse side if necessary and identify by block number)

Single and multimode optical fibers
Optical integrated circuit
Waveguide
Optical couplers
Electrooptic substrates

20. ABSTRACT (Continue on reverse side if necessary and identify by block number)

This report covers the application of integrated optical circuits (IOCs) and fiber optics to Navy and other DoD programs in aircraft, shipboard, and other systems. It explores the feasibility of employing fiber optics and IOC technology in military applications such as high-capacity (multi-GHz) telecommunications and secure (nonradiating and radiation resistant) communication systems.

DD FORM 1 JAN 73 1473 EDITION OF 1 NOV 68 IS OBSOLETE
S/N 0102-014-6601 |

UNCLASSIFIED

SECURITY CLASSIFICATION OF THIS PAGE (When Data Entered)

OBJECTIVE

Study and contribute to the advancement of integrated optical circuits (IOCs) and fiber optics and their application in communication systems. Emphasize applications in Navy and other DoD programs in aircraft, shipboard, and other systems.

Contribute to and evaluate the state of the art in material and device techniques for the fabrication of IOC devices such as couplers, switches, and modulators. Determine the feasibility of employing fiber optics and IOC technology in military applications such as high-capacity (multi-GHz) telecommunications and secure (nonradiating and radiation resistant) communication systems.

RESULTS

1. Single and multimode optical fibers of specialized shapes for optical integrated circuit interface applications have been successfully drawn.

2. Horn-shaped structures, for efficient coupling of light between fibers and optical integrated circuits, have been analyzed and samples fabricated.

3. The mathematical theory of periodically distributed perturbations of optical waveguides has been developed and applied to distributed feedback lasers, couplers, and mode converters.

4. The power requirements for the fabrication of channel optical waveguides in glass by cw laser heating have been characterized experimentally.

RECOMMENDATIONS

1. Develop masking and photolithography for the fabrication of single-mode channel optical waveguides.

2. Develop low-loss single-mode glass fibers, 1–3 km in length.

3. Develop optical interconnections between waveguides, fibers, and lasers.

4. Develop optical integrated circuit elements such as waveguide couplers and electrooptic modulators.

5. Provide continued support to the development of continuous room temperature laser diodes.

6. Develop electronic drivers for electrooptic switches, modulators, and detector amplifiers.

7. Assemble an IOC breadboard demonstration system incorporating the low-loss fibers, laser diodes, and integrated optical circuits developed in this program.

ADMINISTRATIVE INFORMATION

The work reported here was sponsored by the Advanced Research Projects Agency, Material Sciences, Arlington, Virginia, under ARPA Order 2158, Amendment 1; Program Code 3010; Contract F215.01; Element 61101E (NELC F215). Work was performed from 1 October to 30 December 1973. Principal investigator was D. J. Albares of NELC Electro-Optics Technology Division (Code 2500); associate investigators were W. M. Caton, D. B. Hall, W. E. Martin, T. G. Pavlopoulos, and H. F. Taylor of Code 2500, H. H. Wieder of

Electronic Materials Science Division (Code 2600), J. H. Harris of the University of Washington, C. Yeh of the University of California at Los Angeles, and R. B. Wilson of the Hughes Research Laboratories, Malibu, California. This report was authored by Caton and was approved for publication 17 September 1974.

CONTENTS

INTRODUCTION

The fabrication of miniature solid-state optical components and thin-film waveguides to interconnect them on semiconductor or dielectric substrates is becoming feasible with the advancement of such disciplines as the materials sciences, quantum electronics, and guided-wave optics. Integrated optical components – sources, detectors, modulators, and various coupling elements – on one or more tiny substrates will comprise systems much smaller in size and weight than optical systems employing discrete components. The new systems will be much less susceptible to environmental hazards, such as mechanical vibrations, extremes in temperature, and electromagnetic fluctuations, because of their small size and high packaging density. In addition, wideband active components, such as waveguide electrooptic modulators, will be able to operate at very low power levels because of the small dimensions involved.

Integrated optics will perform a number of functions in the area of optical communications. They include rapid modulation and switching by guided-wave elements using applied fields to generate small electrooptic or magnetooptic index changes, coupling, filtering of signals, light detection by p-n junctions or other structures in thin films, and light generation by thin-film laser elements.

Guided-wave optical components have found an important potential use in the area of optical communications because of the recent progress in the fabrication of single-mode fiber-optic waveguides with very low losses. Fiber-optic waveguides with losses as low as 4 dB/km at 0.85-μm and 1.06-μm wavelengths (for GaAs and Nd-YAG lasers, respectively) and with single-mode fibers having anticipated bandwidths as high as 10 GHz for a 1-km length immensely widen the horizon of optical communications. However, devices must be developed to couple energy efficiently with the fibers and to process the optical information efficiently at rates approaching the bandwidth capacity of the fibers.

Another promising area is in fast, high-capacity, high-density multiport switches for interconnecting networks.

Fiber-optic waveguide systems offer significant advantages for military information transfer, both immediately, with discrete components and multimode fibers, and in the future, with single-mode fibers and integrated optical elements. These advantages include freedom from electromagnetic interference (EMI), elimination of grounding problems, and increased security (no signal leakage), as well as the potential for large savings in size, weight, power consumption, and cost. In addition to high-capacity point-to-point communications, a major interest in integrated optics from a military standpoint is the potential for implementing a fiber-optic-transmission-line, multi-terminal (data bus) multiplexing system through low-loss coupling and modulation elements. This will provide isolated-terminal, redundant information transfer, thus facilitating the truly modular (including distributed computer) command control and communications system.

The objective of the program reported here is to advance the material and device physics of integrated optics for military applications, to establish in concert with other Navy and DoD programs a continuing assessment of system requirements and cost benefits for R&D investments in each application area, and to produce prototype optical elements and subsystems that are aimed at satisfying these requirements. The work on the program that was performed at Naval Electronics Laboratory Center (NELC) and on contracts administered by NELC was in the areas of integrated-optical-circuit (IOC) applications assessment, materials for IOC devices and substrates, pattern fabrication, theoretical analysis, components, and system concepts.

Experimentally, effort continued to be centered on the fabrication of IO components, such as optical waveguides and waveguide modulators. The reason for this concentrated effort in novel fabrication methods for optical waveguides and derived structures is that the employment of IOCs will be of practical interest only after inexpensive fabrication techniques have been developed.

I. THEORETICAL ANALYSIS OF DISTRIBUTION NETWORKS AND ELECTRICALLY CONTROLLABLE COUPLERS FOR INTEGRATED OPTICS

Thin-film and channel-waveguide optical couplers will be important integrated optics components. Applications of these couplers in optical networks, modulators, and multiplexers/demultiplexers would be drastically increased if the coupling were dynamically controllable by an electric signal. Electrooptic substrates can be used to control the coupling coefficient between two waveguides, but such a scheme would be inefficient because of the upper limitation on the change of the refractive index of existing materials that could be achieved with a reasonable voltage. A study of the power distributions (in a network of N parallel guides) as a function of the distance from the input plane has shown that electrically controllable couplers are feasible.

SYMMETRIC AND NONSYMMETRIC OPTICAL NETWORKS

Let us consider N identical optical waveguides with K being the coupling coefficient between two neighboring guides. The field E_n in the n^{th} guide is determined by the system of equations:

$$\frac{d E_n}{dz} = - i K E_{n+1} - i K E_{n-1} \quad \text{for } 2 \leq n \leq N-1$$

$$\frac{d E_1}{dz} = - i K E_2$$

$$\frac{d E_N}{dz} = - i K E_{N-1}$$

where we have neglected the direct coupling between nonneighboring guides. If the input light is fed into the m^{th} guide, then the normalized initial condition is:

$$E_n(0) = \begin{cases} 1 \text{ for } n = m \\ 0 \text{ for } n \neq m \end{cases} .$$

The above system of equations can be written in matrix form as follows:

$$\frac{d}{d\xi} \underline{E} = \underline{M} \cdot \underline{E}$$

$$\underline{E}(0) = \underline{c} \ , \qquad (1.1)$$

where $\xi = Kz$ and

$$\underline{E} = \begin{pmatrix} E_1 \\ E_2 \\ \vdots \\ E_N \end{pmatrix} \qquad \underline{c} = \begin{pmatrix} 0 \\ \vdots \\ 1 \\ \vdots \\ 0 \end{pmatrix} \leftarrow m^{th} \text{ element}$$

$$\underline{\underline{M}} = -i \begin{pmatrix} 0 & 1 & 0 & \cdots & 0 \\ 1 & 0 & 1 & \cdots & 0 \\ 0 & 1 & 0 & \ddots & 0 \\ & \ddots & \ddots & \ddots & 1 \\ 0 & & 1 & & 0 \end{pmatrix}$$

Equation (1.1) can be solved by determining the eigenvalues and eigenvectors of the matrix $\underline{\underline{M}}$. For $N \to \infty$, the solution of equation (1.1) are the well known Bessel functions:

$$E_n = (-i)^{|n-m|} J_{|n-m|}(2\xi) \quad .$$

For N finite, the solution can be determined in a straightforward manner with a digital computer. In figure 1.1 we present the power $P_n = E_n E_n^*$ for a number of configurations (N=2, 3, and 5) with different input conditions. These various configurations can be used to perform a number of functions in optical networks. Some of the possible applications are shown in figure 1.2 and discussed below.

Figure 1.2(a) shows an energy transfer function configuration. Complete transfer occurs if the coupling length is an odd integer of $\pi/2K$ (see fig 1.1(b)). Figure 1.2(b) shows an energy divider configuration. The input energy is equally and completely divided between the two outputs if the coupling length is $\pi/2K\sqrt{2}$ (see fig 1.1(c)). An elementary logic system is shown in figure 1.2(c). The two inputs A and B are in phase, and the output is given by the truth table. Figures 1.2(d) and 1.2(c) correspond to energy transfer from two inputs to two outputs, where the useful information is the amplitude or the frequency of the signal (assuming that the two frequencies ω_1 and ω_2 are not very different so that K is approximately the same for both). Figures 1.2(f) and 1.2(g) represent a possible configuration for an electrically controllable coupler or switch which is discussed in the next section.

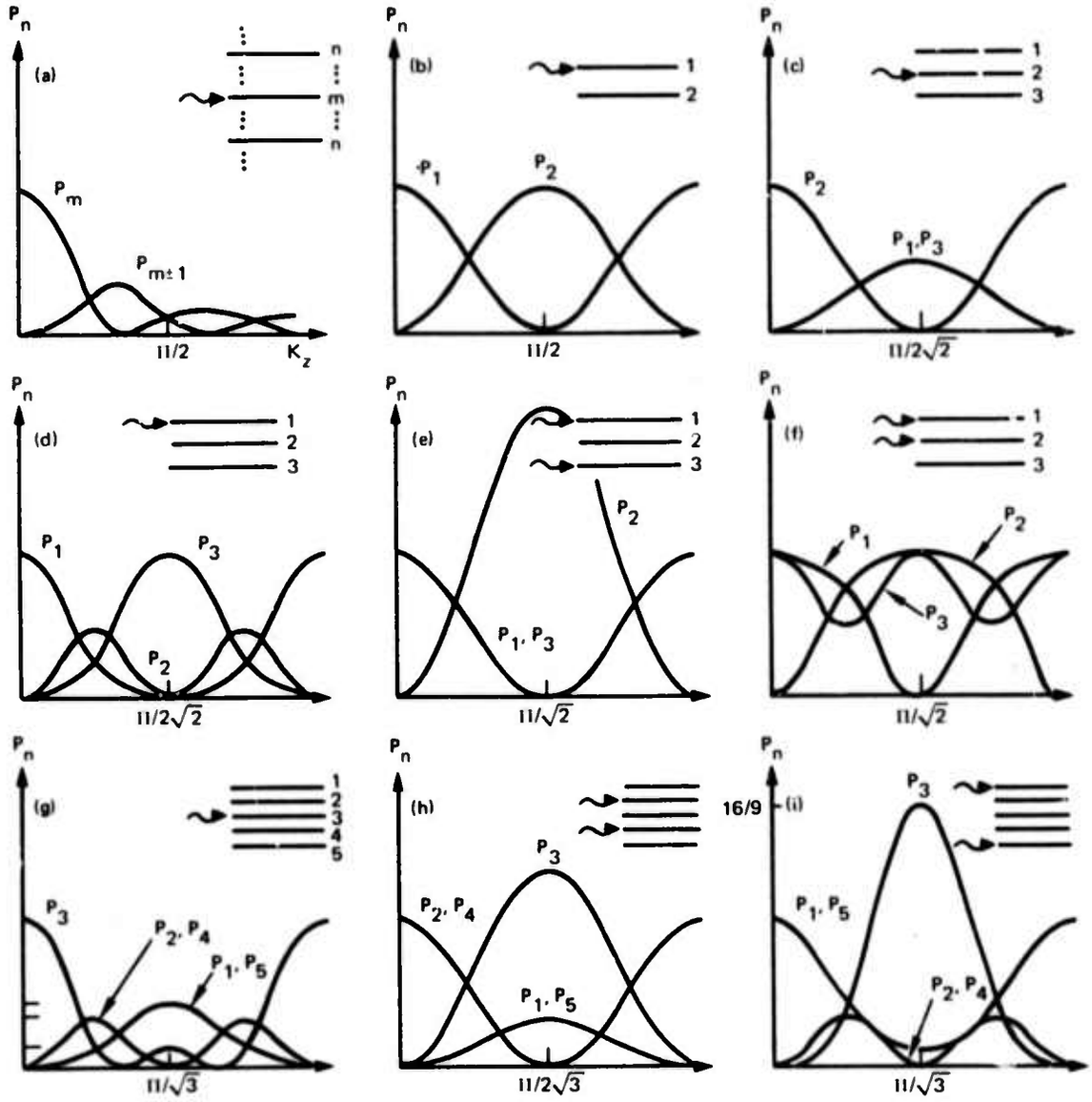

Figure 1.1. Power distribution in coupled optical networks. P_n is the power in the n^{th} guide as a function of the propagation distance z. K is the coupling constant between neighboring guides. Nonneighboring guides are assumed to be uncoupled. For the case where there is more than one input, these inputs are assumed to be in phase.

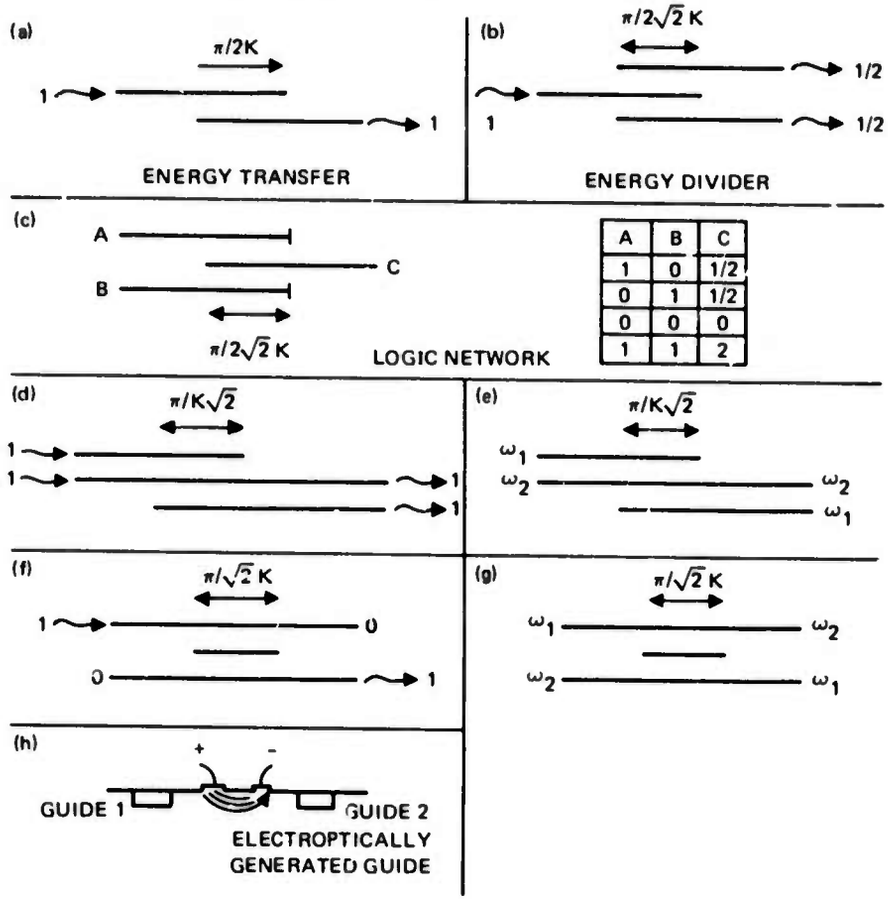

Figure 1.2. Different configurations of optical network which could be used in energy transfer, energy distribution, controlled switching – (see text).

ELECTRICALLY CONTROLLABLE COUPLER

The basic configuration for an electrically controllable coupler (ECC) is shown in figures 1.2(f) and 1.2(h). The two permanent channel guides are imbedded at the surface of an electrooptic substrate. They can be formed by proton bombardment, ion implantation, diffusion, or other techniques. The two guides are so located that the direct coupling is very weak. In the region between the two guides, a third channel of finite length is dynamically generated by applying a voltage to the two electrodes shown in the figure. The resulting electric field generates a local change in the refractive index. This controllable channel plays the role of a bridge between the two permanent guides. The electrodes should be located so that the cross section of the dynamic guide is similar to the cross section of the two permanent guides.

The power distribution as a function of the propagation distance in a three-guide system, where the energy is fed in the first guide, is shown in figure 1.1(d) and is given by (from equation 1.1):

$$P_1(z) = \frac{1}{4}\left[\cos\left(K\sqrt{2}\,z\right) + 1\right]^2 ,$$

$$P_2(z) = \frac{1}{2}\left[\sin\left(K\sqrt{2}\,z\right)\right]^2 ,$$

and

$$P_3(z) = \frac{1}{4}\left[\cos\left(K\sqrt{2}\,z\right) - 1\right]^2 ,$$

where we assume that the direct coupling coefficient K' between the two permanent guides is $\ll K$. Complete energy transfer between the two permanent guides occurs if the controllable channel has a length $L = \pi/K\sqrt{2}$.

In the absence of the bridge channel, the power distribution in the two permanent guides is:

$$P'_1(z) = \cos^2(K'z)$$

and

$$P'_2(z) = \sin^2(K'z) ,$$

and the energy transferred over the length L is

$$\Delta P = \sin^2\left(\frac{\pi}{\sqrt{2}}\frac{K'}{K}\right) .$$

Therefore, the dynamic efficiency of the coupler can be defined as:

$$\eta = 1 - \Delta P = \cos^2\left(\frac{\pi}{\sqrt{2}}\frac{K'}{K}\right) .$$

The analytic expression of the coupling coefficients was derived by Marcatilli* as:

$$K = \frac{2s^2\delta}{s^2 + \delta^2}\,\frac{\exp\left[-\delta(D-a)\right]}{\kappa a}$$

and

$$K' = \frac{2s^2\delta}{s^2 + \delta^2}\,\frac{\exp\left[-\delta(2D-a)\right]}{\kappa a}$$

where "a" is the width of each channel, D is the distance between the center lines, κ and s are respectively the propagation constants along, and perpendicular to, the propagation

*Marcatilli, E. A. J., "Dielectric Rectangular Waveguide and Directional Coupler for Integrated Optics," Bell Sys. Tech. J., v 48, p 2071-2102, September 1969.

direction in the coupler plane, and δ is the exponential fall off between the guides. The above expressions were derived from well-confined modes, but they may be used as a good approximation in the general use. Using the above expressions of K and K′ we can express L and η as:

$$L = \frac{\pi}{2\sqrt{2}} \frac{s^2 + \delta^2}{s^2 \delta} \kappa a \exp\left[\delta(D-a)\right]$$

and

$$\eta = \cos^2\left[\frac{\pi}{\sqrt{2}} \exp\left(-\delta D\right)\right] .$$

We carried out a numerical study of the simplified coupler scheme shown in figure 1.3(a), where the guides are thin-film layers. η_1 is the index of refraction of the substrate and γ is the percentage increase generated when a voltage is applied. γ is also taken as the percentage index increase in the permanent guides. In figure 1.4 η and L/λ are plotted as a function of a/λ for a fixed value of D/a, where λ is the optical wavelength in vacuum. It is clear that high efficiency ($\eta \geq 90\%$) is possible at high frequencies, and larger values of η_1 or γ lead to a wider region of high efficiency. On the other hand, the value of L/λ increases with a/λ. To illustrate, let us choose $\eta_1 = 3.5$, $\gamma = 0.001$, and $\lambda = 1.15\mu$. For an efficiency of 90%, then,

$$a = 2.3\mu, D = 3.45\mu \text{ and } L = 304\mu .$$

An efficiency of 99% can be achieved if

$$a = 2.3\mu, D = 5.1\mu, \text{ and } L = 920\mu .$$

For shorter wavelengths, the above numbers are proportionally smaller. In figure 1.3(b) another scheme for an electrically controllable coupler is shown.

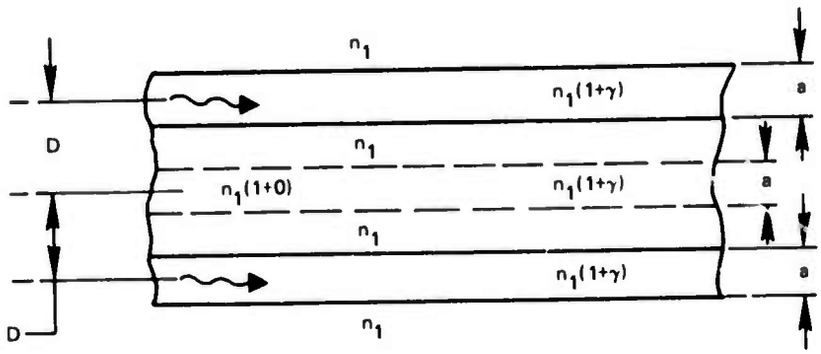

(a)

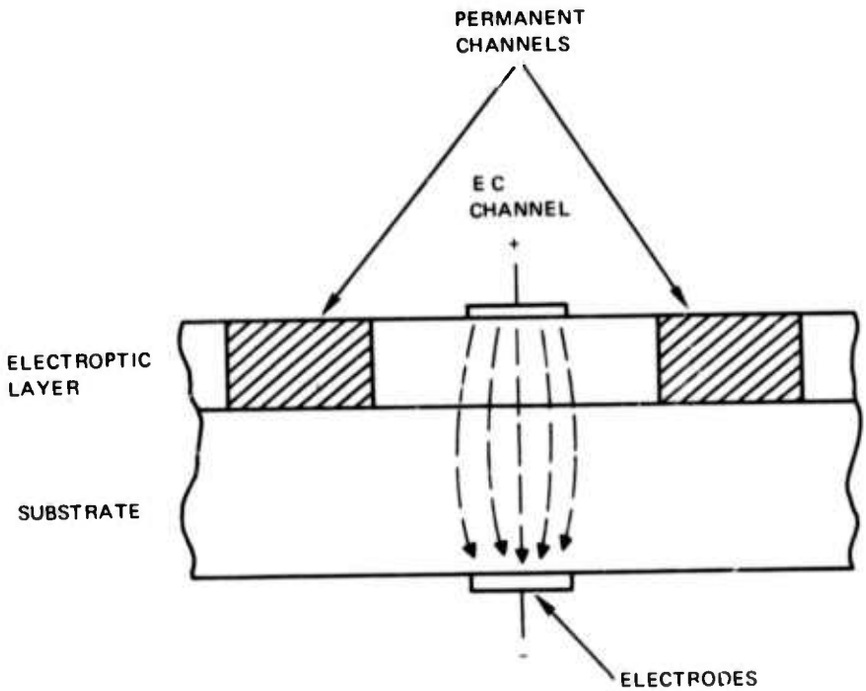

(b)

Figure 1.3. (a) Simplified ECC for thin-film guides. γ is the percentage change of the index of refraction in the permanent guides. γ is also taken as the percentage change due to the electrooptic effect.
(b) Another possible configuration for an ECC.

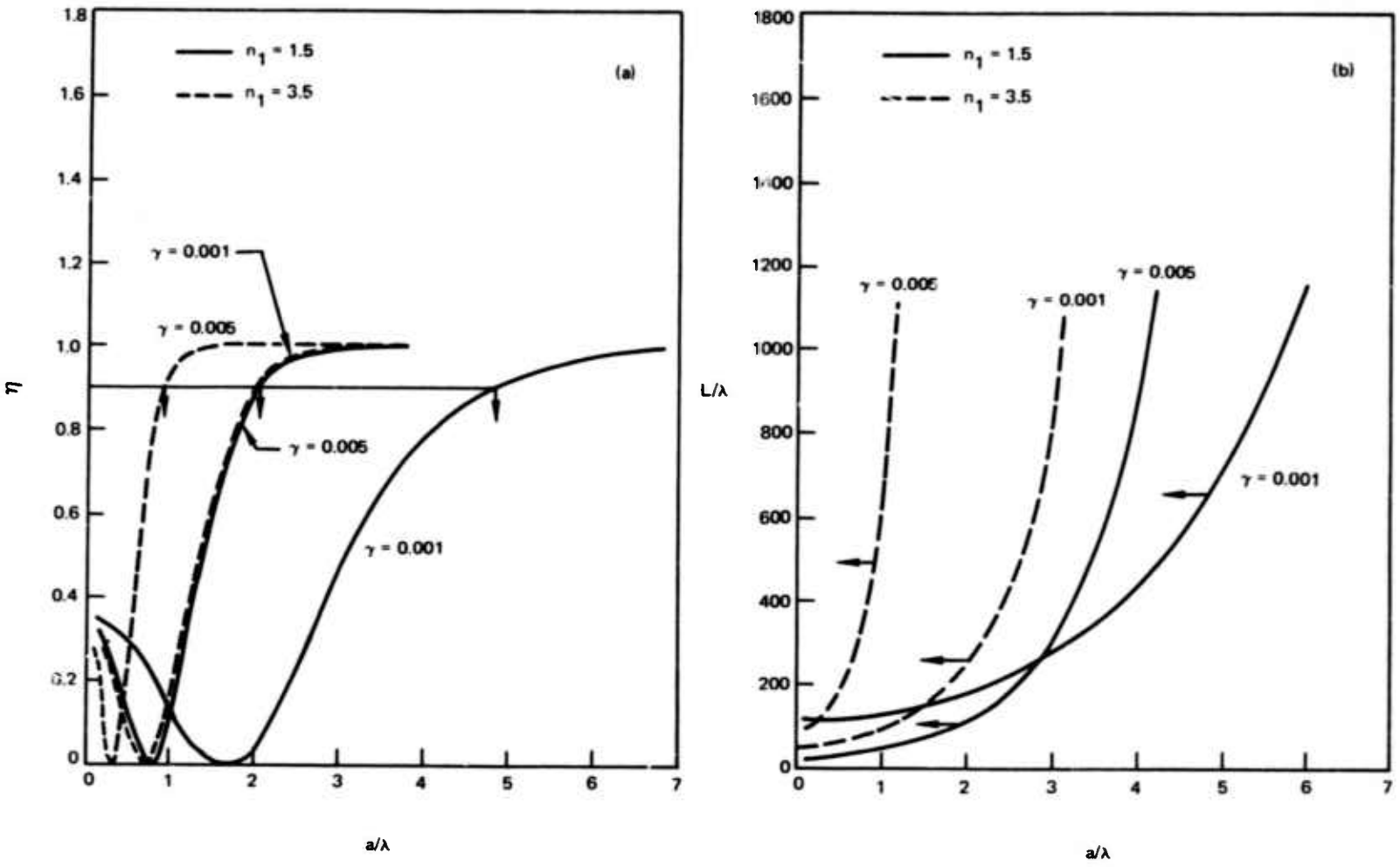

Figure 1.4. Dynamic efficiency and effective length of the ECC shown in figure 1.3(a), as a function of a/λ, for different values of η_1 and γ. The value of D/a is taken equal to be 1.5.

CONCLUSION

The above results show that some simple structures can be used to achieve efficient dynamic switching over relatively short distances. The dynamic coupler may play a central role in complex optical networks and multiplexers/demultiplexers. A scheme for a four-channel multiplexer/demultiplexer is shown in figure 1.5.

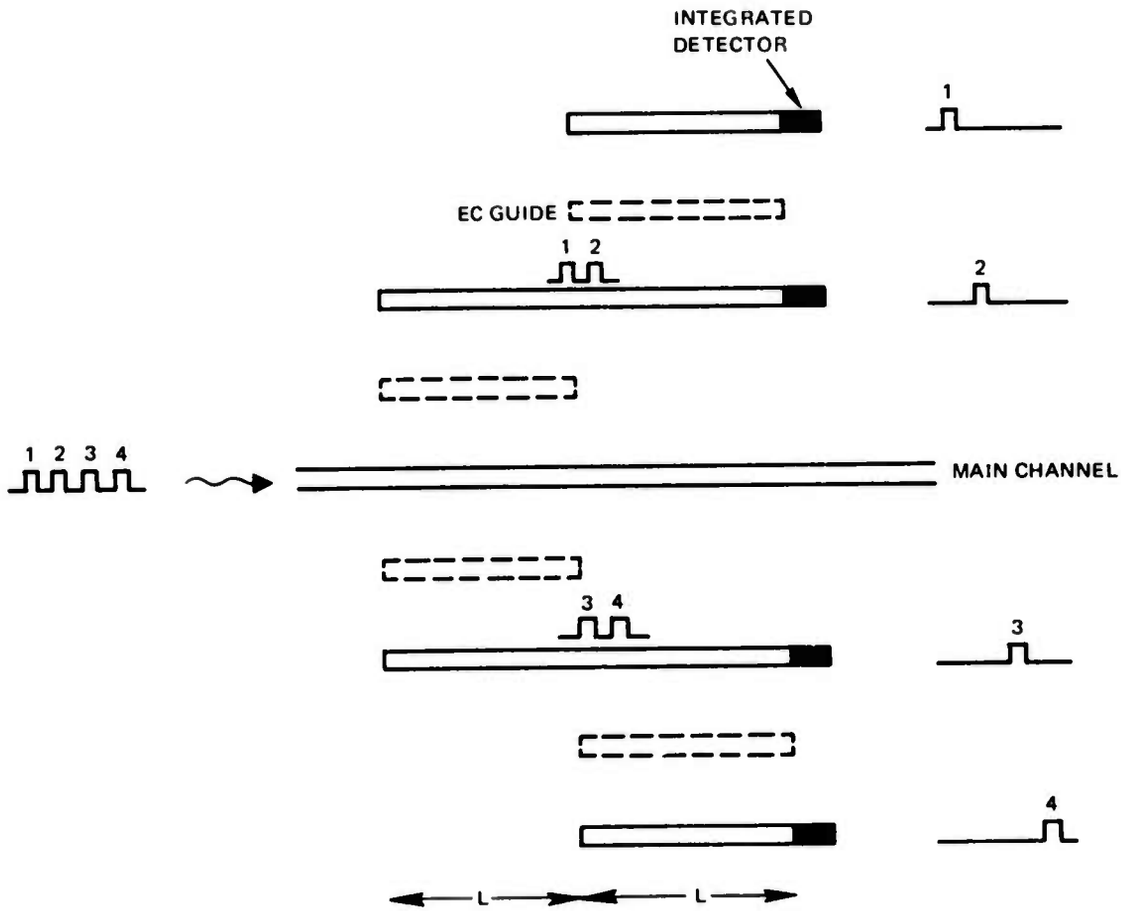

Figure 1.5. Possible configuration for a four-channel optical demultiplexer. The dashed guides are electrically controllable.

2. THEORETICAL INVESTIGATION OF MODE CONVERSION IN PERIODICALLY DISTURBED THIN-FILM WAVEGUIDES

Periodic structures have a wide range of application in active and passive optical thin-film structures. Their stop-band, pass-band characteristic can be used for disturbed feedback, filtering, and coupling. Their space-harmonic characteristic can be mainly used for phase-matched nonlinear interactions and for coupling to drifting electrons in a thin-film semiconductor.

The case of coupling between nonidentical modes has been analyzed for the efficiency of the mode conversion and its use for mode generation, filtering, and distributed feedback. This analysis is applicable to higher-order mode feedback in a DFB (distributed feedback) laser operating on a lower forward mode. Such a scheme is sometimes more efficient than when the feedback and direct waves are in the same mode.

The three important types of periodic structures analyzed are periodically inhomogeneous thin-film guides, periodically inhomogeneous substrate guides, and thin-film waveguides with periodic surfaces. All these structures are technologically feasible.

WAVE SOLUTION AND BRILLOUIN DIAGRAM

Electromagnetic waves can be guided in a structure which consists of a thin-film dielectric of relative permittivity ϵ_1 imbedded in a medium of relative permittivity $\epsilon_2 < \epsilon_1$. For a transverse electric guided wave the field expression is

$$\underline{E} = \underline{e}_y C\, u(x) \exp(i\kappa z) \tag{2.1(a)}$$

$$u(x) = \begin{cases} \cos(sx)/\cos(sL) & \text{(even modes, } |x| \leq L) \\ \sin(sx)/\sin(sL) & \text{(odd modes, } |x| \leq L) \\ \exp(\delta L - \delta|x|) & \text{(even modes, } |x| \geq L) \\ \operatorname{sign}(x) \exp(\delta L - \delta|x|) & \text{(odd modes, } |x| \geq L) \end{cases} \tag{2.1(b)}$$

where 2L is the waveguide thickness, C is the field at the boundary, and s, δ, and κ are the components of the wave vector. These wave vectors are related to the frequency $\omega/2\pi$ by the dispersion relations

$$\kappa^2 + s^2 = \epsilon_1 k^2 , \tag{2.2(a)}$$

$$\kappa^2 - \delta^2 = \epsilon_2 k^2 , \tag{2.2(b)}$$

and

$$\delta = s \begin{cases} \tan sL & \text{(even modes)} \\ -\cot an sL & \text{(odd modes)} \end{cases} , \tag{2.2(c)}$$

where $k = \omega/c$. The above relations have multiple solutions which correspond to the different modes.

If the optical guide is periodic, the field consists of an infinite number of space harmonics of longitudinal wave vectors

$$\kappa_{pn} = \kappa_p + n K , \tag{2.3}$$

where p is the mode index, n is the space-harmonic index, $K = 2\pi/\Lambda$ where Λ is the perturbation period, and κ_p is to be determined. The corresponding Brillouin diagram consists of an infinite number of "subdiagrams," each identical to the diagram of a homogeneous thin-film waveguide. Strong phase-matched coupling occurs at the intersection points between different harmonics, leading to reflection or mode conversion. Two types of coupling could occur:

1. Codirectional, in which the group velocities of the two coupled harmonics are parallel (fig 2.3(a)). In this case the energy is transferred back and forth between the two harmonics.

2. Contradirectional, in which the group velocities are antiparallel (fig 2.3(b)). In this case, there is a one way energy transfer.

MODE CONVERSION IN A PERIODICALLY INHOMOGENEOUS GUIDE

Consider the case of a periodically inhomogeneous guide imbedded in a homogeneous substrate, where

$$\epsilon_1(z) = \epsilon_1(1 + \eta \cos Kz) \qquad \text{with} \quad \eta \ll 1 \tag{2.4}$$

and

$$\epsilon_2 = \text{constant} .$$

Without any loss of generality, we consider the interaction between the n = 0 space harmonic of the p^{th} mode and the neighboring $n = \pm 1$ space harmonics of the q^{th} mode. The phase-matching condition is

$$\kappa_p \pm \kappa_q = K . \tag{2.5}$$

The + and − signs correspond, respectively, to the contradirectional and codirectional interactions. Let ω_{pq} be the frequency at which this condition is satisfied. For η small, all the other space harmonics can be neglected.

To understand and formulate the coupling mechanism, let us consider the p^{th} mode wave of frequency $\omega = \omega_{pq} + \Delta\omega$. The corresponding electric field can be written as

$$E_{po} = C_{po}\, u'_{po}(x) \exp(i\kappa'_p z) , \tag{2.6}$$

where $\kappa'_p = \kappa_p + \Delta\kappa$, and $u'_{po}(x)$ is given by equation (2.1(b)) with s and δ replaced by $s'_p = s_p + \Delta s_p$, and $\delta'_p = \delta_p + \Delta\delta_p$, respectively. The terms κ_p, s_p, and δ_p correspond to the homogeneous guide, and $\Delta\kappa$, Δs_p, and $\Delta\delta_p$ are small perturbations caused by the inhomogeneity. Due to the presence of the periodic component in the dielectric constant (2.3), a spatially periodic convection current J_c is generated:

$$\begin{aligned} J_c &= -i\omega\eta\, \epsilon_0 \epsilon_1 \cos(Kz)\, E_{po} \\ &= -i\omega\eta \frac{\epsilon_0 \epsilon_1}{2} C_{po}\, u'_{po}(x)\, h(x) \left[\exp i(\kappa'_p + K)z + \exp i(\kappa'_p - K)z\right] . \end{aligned} \tag{2.7}$$

where $h(x) = 1$ for $|x| < L$ and $h(x) = 0$ for $|x| > L$. This current will excite the two neighboring space harmonics. Let us consider the case of contradirectional longitudinal phase

matching. Then a backward q^{th} mode wave $E_{q,-1}$ will be excited. However, to determine the effective excitation current for the new q_{th} mode, the current J_e has to be expanded as a function of the transverse modes:

$$u'_{po}(x)\, h(x) = \sum_j a'_{pj}\, u_j(x) \quad , \tag{2.8}$$

and only the term a'_{pj} has to be taken into account. This corresponds to transverse phase matching. The expansion coefficients a'_{pj} are given by

$$a'_{pj} = \frac{\int_{-\infty}^{+\infty} u'_p(x)\, h(x)\, u_j^*(x)\, dx}{\int_{-\infty}^{+\infty} u_j(x)\, u_j^*(x)\, dx} = \frac{\int_{-L}^{+L} u'_p(x)\, u_j^*(x)\, dx}{\int_{-\infty}^{+\infty} u_j(x)\, u_j^*(x)\, dx} . \tag{2.9}$$

Now the corresponding wave equation is

$$\left[\frac{\partial^2}{\partial x^2} + \frac{\partial^2}{\partial z^2} + \epsilon_1 \frac{\omega^2}{c^2}\right] E_{q,-1} = -\eta \frac{\omega^2}{2} \frac{\epsilon_1}{c} C_{po}\, a'_{pq}\, u_q(x)\, e^{i(\kappa'_p - K)z} \tag{2.10}$$

for $|x| < L$, and for $|x| > L$ we replace ϵ_1 by ϵ_2 in the parentheses. Replacing $E_{q,-1}$ by an expression similar to equation (2.6), we get

$$\left[(s_q + \Delta s_q)^2 + (\kappa_q + \Delta\kappa)^2 - \epsilon_1 \frac{\omega^2}{c^2}\right] C_{q,-1}\, u'_q(x)$$

$$= \eta \frac{\omega^2}{2} \frac{\epsilon_1}{c^2} C_{po}\, a'_{pq}\, u_q(x)\, e^{i(\kappa'_p + \kappa'_q - K)z} \tag{2.11}$$

for $|x| < L$ and

$$\left[-(\delta_q + \Delta\delta_q)^2 + (\kappa_q + \Delta\kappa)^2 - \epsilon_2 \frac{\omega^2}{c^2}\right] C_{q,-1}\, u'_q(x)$$

$$= \eta \frac{\omega^2}{2} \frac{\epsilon_1}{c^2} C_{po}\, a'_{pq}\, u_q(x)\, e^{i(\kappa'_p + \kappa'_q - K)z} \tag{2.12}$$

for $|x| > L$. Using the dispersion relation for the unperturbed case (2.2), neglecting second-order terms (small term x u'_q = small term x u_q), and expressing Δs_q and $\Delta\delta_q$ as functions of $\Delta\kappa_q$ and $\Delta\omega$ by differentiating equations (2(a)–2(c)), equations (2.12) and (2.13) reduce to:

$$\left[-\frac{\Delta\kappa}{\kappa_q} + B_q \frac{\Delta\omega}{\omega_{pq}}\right] C_{q,-1} = \eta \frac{\epsilon_1}{4} \left(\frac{\omega}{c\kappa_q}\right)^2 a_{pq}\, C_{p,0} \quad . \tag{2.13}$$

where, for the even modes:

$$B_q = \left(\frac{\omega_{pq}}{c\kappa_q}\right)^2 \left[\epsilon_1 \frac{\delta_q L + \sin^2(s_q L)}{\delta_q L + 1} + \epsilon_2 \frac{\cos^2(s_q L)}{\delta_q L + 1}\right]$$

and

$$a_{pq} = - \frac{\int_{-L}^{+L} u_p u_q^*}{\int_{-\infty}^{+\infty} u_q u_q^*} = \begin{cases} \dfrac{2\delta_q \cos^2(s_q L)}{(\delta_p + \delta_q)(1 + \delta_q L)} & p \neq q \\ \dfrac{\delta_p L + \sin^2(s_p L)}{1 + \delta_p L} & p = q \end{cases} .$$

For the odd modes, the sines and cosines must be exchanged.

At the same time, the q^{th} mode generates a convection current which excites the p^{th} mode; therefore, the coefficients $C_{q,-1}$ and $C_{p,0}$ are also related by

$$\left[-\frac{\Delta\kappa}{\kappa_p} + B_p \frac{\Delta\omega}{\omega}\right] C_{p,0} = \eta \frac{\epsilon_1}{4} \left(\frac{\omega}{c\kappa_p}\right)^2 a_{qp} C_{q,-1} \quad . \tag{2.14}$$

where B_p and a_{qp} are equivalent to B_q and a_{pq} with p and q interchanged. Thus, to satisfy equations (2.14) and (2.15), we must have

$$X = (\alpha_p - \alpha_q) Y \pm \sqrt{(\alpha_p + \alpha_q)^2 Y^2 - \eta^2 \gamma_{pq}^2} \quad . \tag{2.15}$$

where

$$X^+ = \Delta\kappa_p / K \; ; \; X^- = \Delta\kappa_q / K \; , \qquad Y = \Delta\omega/\omega_{pq}$$

$$\alpha_i = -\frac{|\kappa_i|}{2K} B_i \quad \text{with } i = p, q \; ,$$

$$\gamma_{pq} = \frac{\epsilon_1}{4} \left(\frac{\omega}{c}\right)^2 \frac{1}{K} \sqrt{\frac{a_{pq}\, a_{qp}}{|\kappa_p\, \kappa_q|}} \; ,$$

and

$$\kappa_q = - |\kappa_q| \; .$$

The term X corresponds to the normalized change of the longitudinal wave vector when the operating frequency is equal to $\omega_{pq}(1 + Y)$. The characteristic of the above solution is that the longitudinal wave vector is complex in a frequency band (called stop band) centered at ω_{pq} and of total width

$$\Omega = 2\eta\, \omega_{pq}\, \gamma_{pq} / (\alpha_p + \alpha_q) \; , \tag{2.16}$$

and the imaginary component of the wave vector has a maximum equal to

$$M = \eta K \gamma_{pq} \; . \tag{2.17}$$

The corresponding Brillouin diagram is shown in figure 2.1(b). In figures 2.2 and 2.3 we plotted the two parameters Ω/ω_{pq} and $1/M\lambda$ as a function of L/λ for mode conversion (or mode coupling) from the forward basic mode to the backward basic and second even ($p = 2$) modes. λ is the wavelength in vacuum.

As would be expected from physical reasoning, the value of $1/M\lambda$ (attenuation or coupling length) is large near cut-off because most of the energy is in the substrate where no coupling occurs. As the frequency increases, more optical energy is enclosed into the periodic guide leading to stronger coupling ($1/M\lambda$ smaller). This trend continues for the 0-0 modes coupling. However, for the 0-2 modes coupling, after a certain optimal frequency, $1/M\lambda$ starts increasing again because, at high frequencies, the overlap term a_{pq} goes to zero, leading to weaker coupling. The coupling bandwidth behaves in a reverse manner. It should be pointed out that no coupling occurs between an even and an odd mode because a_{pq} vanishes.

In the case of codirectional interaction, the solution for X is

$$X = (\alpha_p + \alpha_q)\, Y \pm \sqrt{(\alpha_p - \alpha_q)^2\, Y^2 + \eta^2\, \gamma_{pq}^2} \qquad (2.18)$$

and the corresponding diagram is shown in figure 2.3(a). In this case there is no stop band, but the energy is transferred back and forth between the two modes. The characteristic energy transfer length T_{pq} is given by

$$T_{pq} = \pi/2M \quad ,$$

which can be determined from figures 2.2 and 2.3.

If only one boundary is perturbed, then the above results are still valid with η replaced by $\eta/2$. However, in this case, even-odd coupling can also occur.

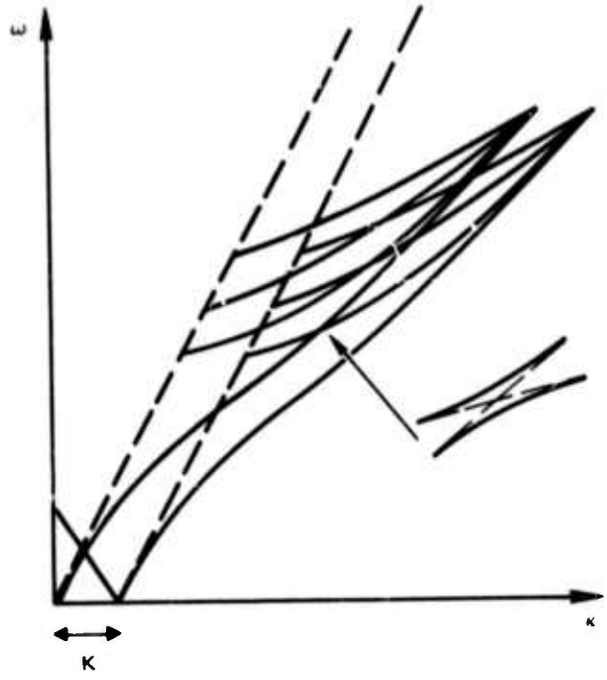

(a)

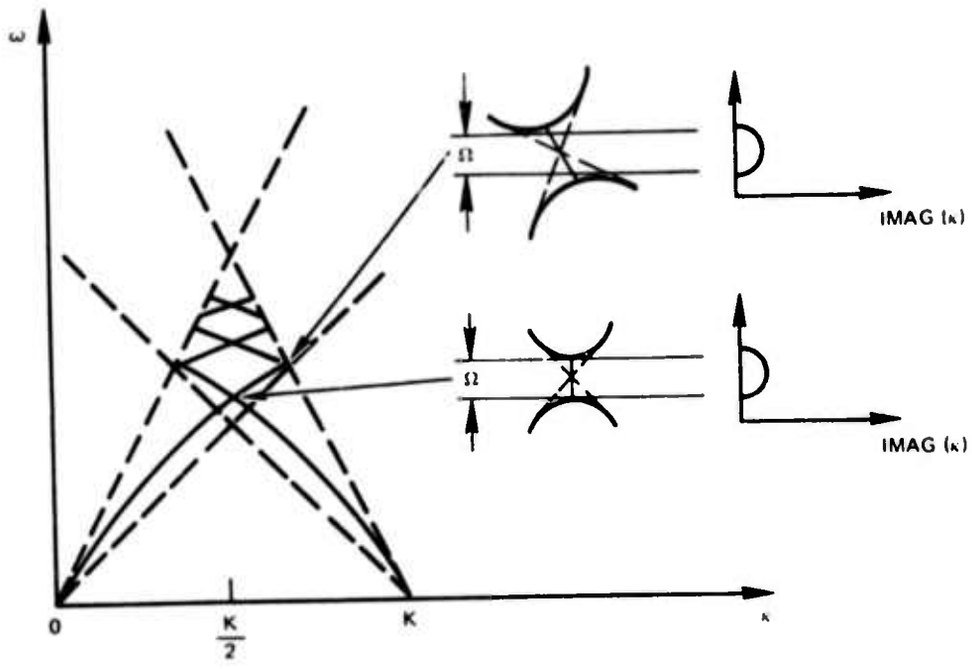

(b)

Figure 2.1. Interaction regions between two space harmonics: (a) codirectional interaction; (b) contradirectional symmetric and nonsymmetric interaction.

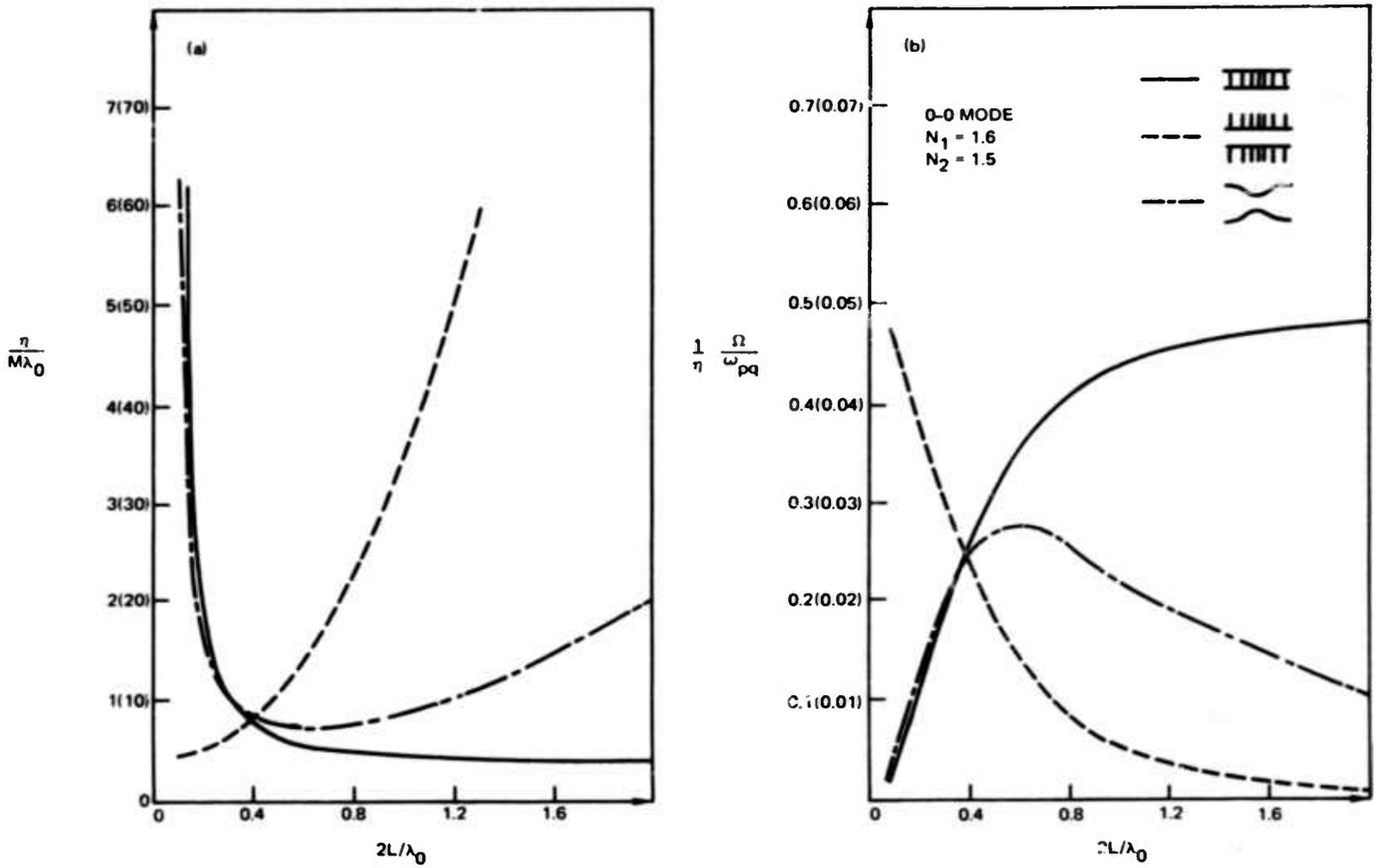

Figure 2.2. Normalized interaction length and bandwidth for the 0-0 modes interaction. The scale in parentheses corresponds to the surface corrugation case.

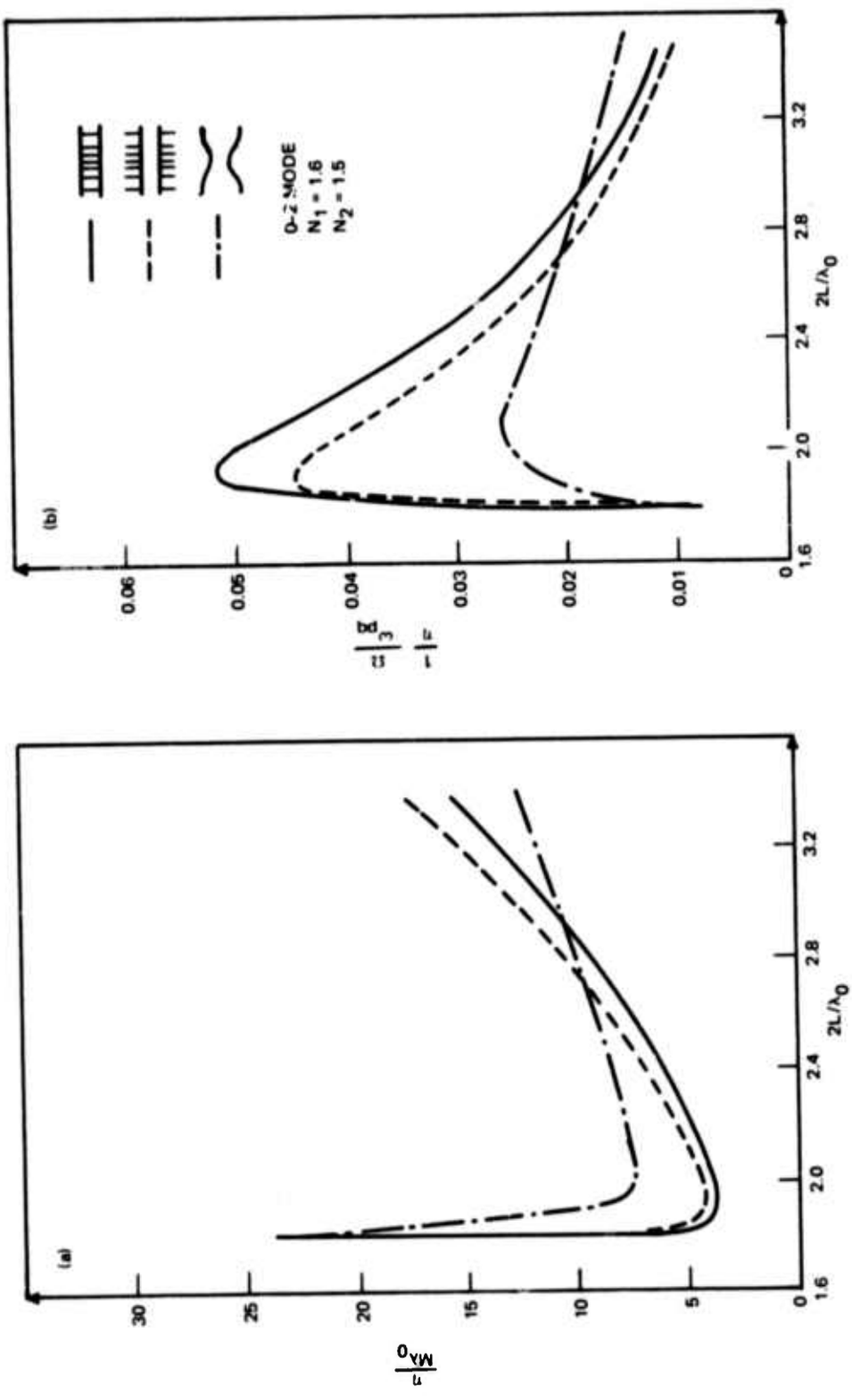

Figure 2.3. Normalized interaction length and bandwidth for the 0-2 modes interaction.

MODE CONVERSION IN A HOMOGENEOUS WAVEGUIDE WITH A PERIODIC SUBSTRATE

The same method used above can also be applied to the case in which the waveguide is homogeneous and the substrate has a periodic dielectric constant. In this case, the source convection current is in the substrate, and equations (2.16) and (2.19) are valid with γ_{pq} replaced by

$$\Gamma_{pq} = \frac{\epsilon_2}{4}\left(\frac{\omega}{c}\right)^2 \frac{1}{K}\sqrt{\frac{b_{pq}\, b_{qp}}{|\kappa_p\, \kappa_q|}} \quad , \tag{2.19}$$

where

$$b_{pq} = \frac{\displaystyle\int_{-\infty}^{-L} u_p u_q^* + \int_{L}^{+\infty} u_p u_q^*}{\displaystyle\int_{-\infty}^{+\infty} u_q u_q^*} = \frac{2\delta_q \cos^2(s_q L)}{(\delta_p + \delta_q)(1 + \delta_q L)} \quad .$$

We remark that for $p \neq q$:

$$\Gamma_{pq} = \frac{\epsilon_2}{\epsilon_1}\gamma_{pq} \quad . \tag{2.20}$$

This is an important result, because it means that for ϵ_2 very close to ϵ_1, the coupling between different modes does not depend appreciably on the fact that the periodicity is in the guide or the substrate. In figures 2.2 and 2.3 we plotted the corresponding values of Ω/ω_{pq} and $1/M\lambda$. For the 0-0 coupling, $1/M\lambda$ increases with the frequency, because the energy tends to concentrate into the guide leading to weak coupling. In the case of the 0-2 interaction, the coupling is also weak ($1/M\lambda$ large) near the mode 2 cut-off, because its energy is very thinly spread into the substrate, and the overlap integral b_{pq} with the 0 mode is very small.

MODE CONVERSION IN A HOMOGENEOUS GUIDE WITH A PERIODIC BOUNDARY

The coupling strength and bandwidth have been determined by using an excitation surface current to represent the surface perturbation.

Consider the p^{th} mode wave of frequency $\omega = \omega_{pq} + \Delta\omega$. From Maxwell's equations

$$\int_{\ell} \underline{H} = -i\epsilon_0 \epsilon_1 \omega \int_s \underline{E} \quad . \tag{2.21}$$

The surface perturbation is equivalent to a surface current, J_s, on a straight boundary, which is related to the fields by

$$\int_{\ell} \underline{H} = -i\epsilon_0 \epsilon_2 \omega \int_s \underline{E} + \int_s \underline{J}_s \quad . \tag{2.22}$$

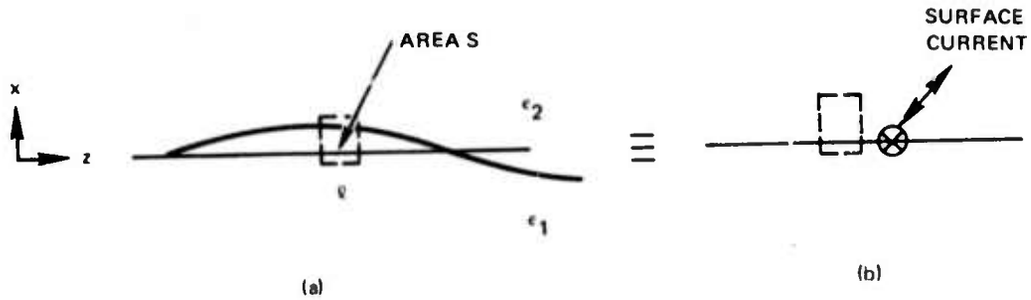

Figure 2.4. A surface perturbation could be replaced by a surface current.

The above two equations imply that

$$\int_S \underline{J}_s = -i\epsilon_0(\epsilon_1 - \epsilon_2)\omega \int_S \underline{E} \Rightarrow$$

$$J_s \Delta z = -i\epsilon_0(\epsilon_1 - \epsilon_2)\omega \Delta x \Delta z E\Big|_{x=L} ,$$

which gives the value of J_s (using $\Delta x = \eta L \cos Kz$)

$$J_s = -i\epsilon_0 \eta L(\epsilon_1 - \epsilon_2)\omega \cos(Kz) C_{po} e^{i\kappa'_p z} . \tag{2.23}$$

This surface current could be phase-matched with the neighboring space harmonics. For the case of contradirectional phase matching (2.8), a backward q^{th} mode is excited. The boundary condition for this new mode is

$$H_z(x = L^+) - H_z(x = L^-) = J_{s1} , \tag{2.24}$$

where J_{s1} is the component in phase with the generated wave. The above equation gives

$$|s'_q \tan(s'_q L) - \delta'_q| C_{q,-1} = \eta \frac{\epsilon_1 - \epsilon_2}{2} L \left(\frac{\omega_{pq}}{c}\right)^2 C_{po} \tag{2.25}$$

for the even modes. For the odd modes, the tangent must be replaced by minus cotangent. At the same time, the q^{th} mode excites the p^{th} mode, leading to a relation similar to equation (2.25) (with p and q exchanged), which then implies that

$$|s'_q \tan s'_q L - \delta'_q| \, |s'_p \tan s'_p L - \delta'_p| = \left(\eta \frac{\epsilon_1 - \epsilon_2}{2} L\right)^2 \left(\frac{\omega_{pq}}{C}\right)^4 . \tag{2.26}$$

This relation replaces the boundary condition (2.2(c)) of the homogeneous guide, and couples the two modes through the perturbation of the boundary. The other dispersion relations (2.2(a)) and (2.2(b)) are still valid.

Replacing s', δ', and κ' by their expressions and following the same method as previously, we find that equation (2.16) is still valid with γ_{pq} replaced by

$$\gamma'_{pq} = \frac{\epsilon_1 - \epsilon_2}{2} \left(\frac{\omega}{C}\right)^2 \frac{1}{K} \sqrt{\frac{d_p d_q}{|\kappa_p \kappa_q|}} . \tag{2.27}$$

where

$$d_i = \frac{\delta_i L \cos^2 (s_i L)}{1 + \delta_i L} \qquad i = p, q \quad .$$

For an odd mode, the cosine should be replaced by sine. This result is identical to the one derived by using the exact Floquet solution.

In a symmetrically perturbed waveguide, only even-even and odd-odd couplings occur. Even-odd couplings occur in the antisymmetric case. If only one boundary is perturbed, all types of coupling are possible.

In figures 2.2, 2.3, and 2.5 $\eta/M\lambda$ and $\Omega/\eta\omega_{pq}$ are plotted for the 0-0, 0-1, and 0-2 modes coupling. Near cut-off, where most of the energy is spread in the substrate, the coupling is weak. The same happens at high frequency, when most of the energy is inside the guide and the field is small at the boundary. The strongest coupling (and therefore feedback or filtering) occurs at an optimum frequency somewhere in between.

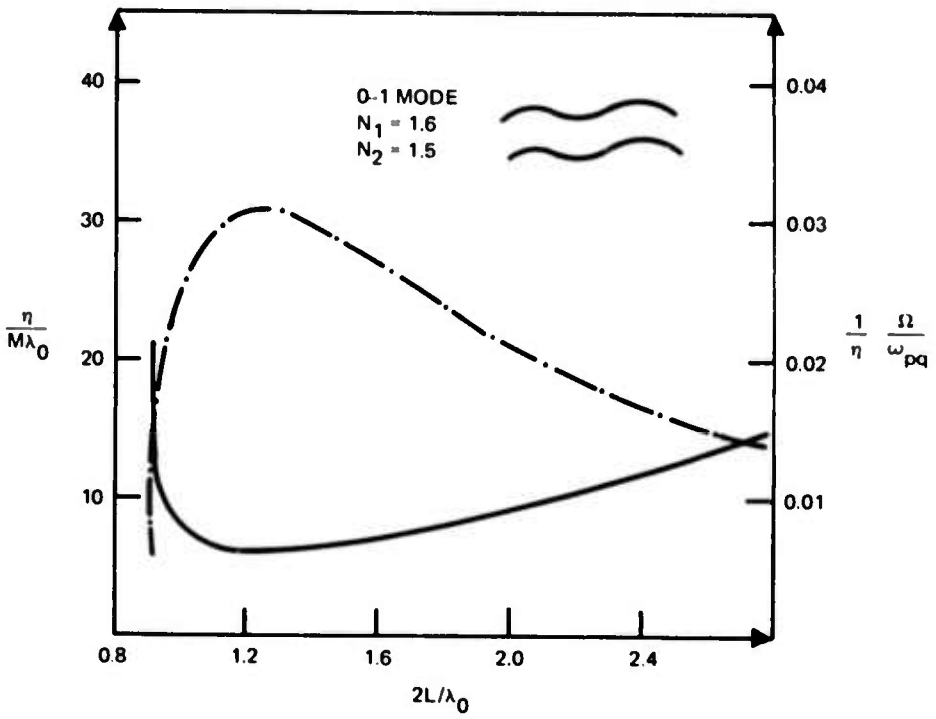

Figure 2.5. Normalized interaction length and bandwidth for the 0-1 modes interaction in an antisymmetrically corrugated guide.

APPLICATIONS AND CONCLUSION

The results of this analysis can be applied to the design of integrated optic filters and distributed feedback lasers. The terms η/M_{pq} and Ω_{pq} describe the coupling, filtering, and feedback efficiencies. The coupling coefficient can be used to determine the gain threshold of a thin-film distributed feedback laser. It is clear that for an optimum design, the operating frequency has to be selected in a well specified region. It should be pointed out that the product

$$\left(\frac{\Omega}{\omega_{pq}}\right)\left(\frac{1}{M\lambda}\right) = \frac{2}{\lambda\,(\alpha_p + \alpha_q)} \tag{2.28}$$

is the same for all three structures studied and depends only on the properties of the unperturbed guide and the operating frequency. This implies that if a structure is designed for a large coupling coefficient, then its bandwidth will be very narrow and vice versa.

The above results can be easily generalized to any type of periodicity which can be expanded in a Fourier series if η is replaced by the coefficient of the Fourier component used for phase matching.

3. ELECTROMAGNETIC THEORY OF BOUNDED DFB LASERS

Great interest has recently been generated in the use of distributed feedback (DFB) cavities in laser systems. Since the development of the first DFB laser in 1971, most investigations have been directed toward thin-film integrated optics sources. However, the use of the DFB cavity in other types of lasers can have major advantages because it would eliminate the need for mirrors, which are one of the major problems in the design of high-power lasers (because of mirror burning) and ultra-high-frequency lasers (because of mirror low reflectivity).

In this analysis we study the interaction of electromagnetic waves with transversely bounded, active, periodic structures which can be used for DFB lasers. We study the coupling between different guided modes and take into account their "effective" gain. The lasing threshold gain and the longitudinal field distribution are derived and discussed for a number of different laser configurations. Specifically, thin-film lasers, diffuse lasers, fiber lasers, and capillary lasers with inhomogeneous cladding (fig 3.1) are considered and it is shown that there are optimum designs for which the gain required for self-sustained oscillation is at a minimum. Periodic index and surface perturbation distributed feedback are covered. Finally we discuss the applications of the above structures and, more generally, of the DFB concept in the fields of planar integrated optics, optic fiber communication, high-power lasers, UV lasers, and possibly X-ray lasers.

To avoid excessive mathematical derivations, we limit our study to the case of TE waves for both planar and circular configurations; however, the approach is directly applicable to TM, HE, and EH modes. An $e^{-i\omega t}$ time dependence is assumed.

THRESHOLD AND LONGITUDINAL FIELD DISTRIBUTION

In principle, a periodic structure supports an infinite number of space harmonics. However, for the case of small periodic perturbations, the coupled-mode theory can be applied near the Bragg frequencies where only the two phase-matched interacting waves have significant amplitudes. The first-order Bragg phase-matching condition for feedback is

$$\beta_p + \beta_q = 2\pi/\Lambda \quad , \tag{3.1}$$

where β_p and β_q are the longitudinal wave vectors of the coupled p^{th} and q^{th} modes, and Λ is the period of the perturbation. Let ω_{pq} be the corresponding frequency.

If the operating frequency ω is very close to ω_{pq} ($\omega = \omega_{pq} + \Delta\omega$), then the coupled-wave equations for the forward p^{th} mode wave

$$F_p(z)e^{i\beta_p z}$$

and backward q^{th} mode wave

$$B_q(z)e^{i\beta_q z}$$

are:

$$+\frac{dF_p}{dz} - (C_p g + i\Delta\beta_p) F_p = i\chi_{pq} B_q \tag{3.2}$$

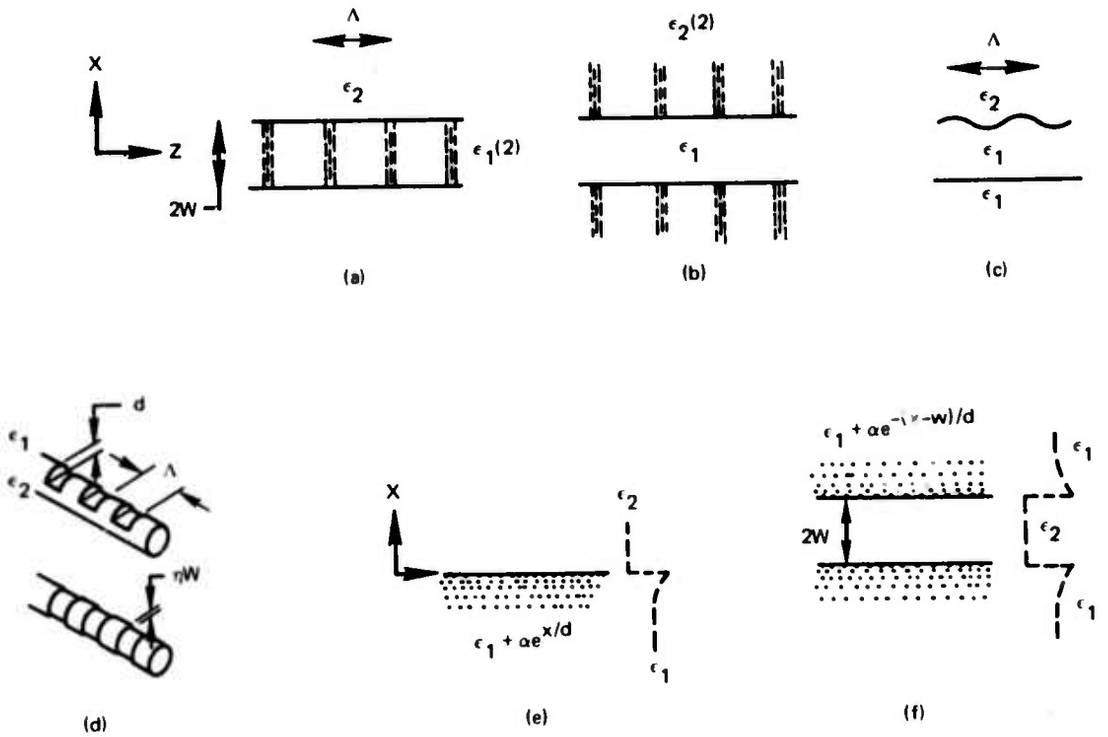

Figure 3.1. Bounded DFB laser structures studied. (a) Thin-film DFB laser with a periodic guide index. (b) Thin-film DFB laser with a periodic substrate index. (c) Thin-film DFB laser with a periodic surface corrugation. The cases of one-boundary and both-boundaries corrugation were considered. (d) DFB fiber laser. The upper configuration can be generated by particle beam machining of a fiber. The lower configuration is harder to achieve; however, it can be treated analytically and is equivalent to the upper one (see text). (e) Diffuse DFB laser. The distributed feedback can be generated by corrugating the surface, and guiding is achieved because of the inhomogeneity. (f) Diffuse capillary DFB laser. Only the planar structure is considered.

and

$$-\frac{dB_q}{dz} - (C_q g + i\Delta\beta_q) B_q = i \chi_{pq} F_p \quad , \tag{3.2}$$

where C_p and C_q are the gain efficiency coefficients ($C_p, C_q < 1$), g is the medium gain (see Gain Efficiency Coefficient), χ_{pq} is the coupling coefficient which takes into account the transverse phase matching (see Coupling Coefficient), and $\Delta\beta_p$ and $\Delta\beta_q$ are related to $\Delta\omega$ by

$$\Delta\beta_p = \psi_p \Delta\omega = \left.\frac{\partial\beta_p}{\partial\omega}\right|_{\omega_{pq}} \Delta\omega$$

and (3.3)

$$\Delta\beta_q = \psi_q \Delta\omega = \left.\frac{\partial\beta_q}{\partial\omega}\right|_{\omega_{pq}} \Delta\omega \quad ,$$

where ψ_p and ψ_q are inversely proportional to the slopes of the Brillouin diagram (group velocity) of the unperturbed guide at ω_{pq}.

The general solution of the coupled-wave equation (3.2) is of the form:

$$F_p = f_1 e^{\gamma z} + f_2 e^{\gamma' z}$$

$$B_q = b_1 e^{\gamma z} + b_2 e^{\gamma' z} \quad , \tag{3.4}$$

and, as the DFB laser is self-oscillating, the following boundary conditions, in the case of no end reflections, must be satisfied:

$$F_p(-L/2) = B_q(L/2) = 0 \quad , \tag{3.5}$$

where L is the laser length. Replacing F_p and B_q in equation (3.2) by their expressions in (3.4) and using the boundary conditions (3.5), we find:

$$\gamma, \gamma' = \frac{C_p - C_q}{2} g + i \frac{\psi_p - \psi_q}{2} \Delta\omega \pm \left[\left(\frac{C_p + C_q}{2} g + i \frac{\psi_p + \psi_q}{2} \Delta\omega \right)^2 + \chi_{pq}^2 \right]^{1/2} \quad , \tag{3.6}$$

$$\frac{\gamma - \gamma'}{2} = \pm i \chi_{pq} \sinh \frac{\gamma - \gamma'}{2} L \tag{3.7}$$

$$F_p = 2 f_1 \sinh \left[\frac{\gamma - \gamma'}{2} \left(z + \frac{L}{2} \right) \right] \exp \left(\frac{\gamma + \gamma'}{2} z - \frac{\gamma - \gamma'}{4} L \right) , \tag{3.8}$$

and

$$B_q = \pm 2 f_1 \sinh \left[\frac{\gamma - \gamma'}{2} \left(z - \frac{L}{2} \right) \right] \exp \left(\frac{\gamma + \gamma'}{2} z - \frac{\gamma - \gamma'}{4} L \right) \quad . \tag{3.9}$$

Equations (3.6) and (3.7) relate the coupling coefficient, threshold gain, and laser length. Equations (3.8) and (3.9) give the longitudinal field distribution. We remark that:

$$\frac{\gamma - \gamma'}{2} = D = \left[\left(\frac{C_p + C_q}{2} g + i \frac{\psi_p + \psi_q}{2} \Delta\omega \right)^2 + \chi_{pq}^2 \right]^{1/2} \tag{3.10}$$

$$\frac{\gamma + \gamma'}{2} = S = \frac{C_p - C_q}{2} g + i \frac{\psi_p - \psi_q}{2} \Delta\omega \quad . \tag{3.11}$$

In the case of coupling between two identical modes ($p = q$), we get $\gamma' = -\gamma$ and

$$\gamma = \left[(C_p g + i \psi_p \Delta\omega)^2 + \chi_{pq}^2 \right]^{1/2} \quad .$$

We remark that the threshold condition (3.7) in the case of $p \neq q$ depends on

$$\frac{C_p + C_q}{2}$$

and

$$\frac{\psi_p + \psi_q}{2} \Delta\omega .$$

However, this is not true for the longitudinal field distribution, which is proportional to:

$$\begin{aligned} I(z) &= \left[F_p(z) + B_q(z)\right]\left[F_p(z) + B_q(z)\right]^* \\ &= A \cosh\left[\left(C_p - C_q\right) g z\right] \left\{ \left|\sinh\left(Dz + D\frac{L}{2}\right)\right|^2 \right. \\ &\quad \left. + \left|\sinh\left(Dz - D\frac{L}{2}\right)\right|^2 \right\} \end{aligned} \tag{3.12}$$

where A is a normalized parameter which is a function of the transverse (or radial) coordinate.

Both the p and q modes are excited in the forward and backward directions. Thus, usually there are two independent sets of coupled waves: forward p coupled to a backward q, and a backward p coupled to a forward q.

The solution for equation (3.7) is multivalued, leading to different longitudinal modes. These modes correspond to the laser spectrum. As will be seen later, the first longitudinal mode does not oscillate exactly at the Bragg frequency because the reflected wave is shifted by $\pi/2$ relative to the original wave, and the double-reflected wave is out of phase with the original one.

COUPLING COEFFICIENT

The coupling coefficient χ_{pq} can be derived by solving exactly the wave equation and taking into account all the space harmonics. However, in the case of a small periodic disturbance, a simple perturbation method gives the same results as the exact solution.

Consider a guided wave propagating in the unperturbed guide. The normalized electric field can be expressed in the form

$$E(x, z) = u(x) \exp(i\beta z) \quad , \tag{3.13}$$

where $u(x)$ is the transverse distribution, which is completely determined by the guide configuration and the transverse wave vectors in the guide s and the cladding (or substrate) δ. The wave vectors β, s, and δ are related to the operating frequency by the dispersion relations for the appropriate waveguide. Let ϵ_1, ϵ_2 be the relative dielectric constants of the guide and the cladding, and 2W the width (or diameter) of the guide. The dispersion relations usually have many solutions which correspond to the different guided modes.

If any of the parameters ϵ_1, ϵ_2, or w is periodically perturbed so that

$$(\epsilon_1, \epsilon_2, w) = (\epsilon_1, \epsilon_2, w)\,[1 + \eta\cos(2\pi z/\Lambda)] \tag{3.14}$$

with $\eta << 1$, then a p^{th} mode wave

$$u_p(x)e^{i\beta_p z}$$

would generate a displacement current J_c or surface current J_s of different longitudinal wave vector:

$$J_{c,s} \sim \eta \begin{pmatrix} \epsilon_1\, u_p(x) \\ \epsilon_2\, u_p(x) \\ w\ \ u_p(w) \end{pmatrix} e^{i\beta_p z} \cos\left(\frac{2\pi}{\Lambda} z\right)$$

$$\sim e^{i\left(\beta_p + \frac{2\pi}{\Lambda}\right)z} + e^{i\left(\beta_p - \frac{2\pi}{\Lambda} z\right)} \quad . \tag{3.15}$$

Any of the two components of the perturbation current could be longitudinally phased matched with, and therefore be a source current for, a backward mode q which satisfies the condition

$$\beta_p \pm \beta_q = 2\pi/\Lambda \quad . \tag{3.16}$$

The (+) sign corresponds to contradirectional (or feedback) coupling and the (−) sign corresponds to the codirectional coupling. Only the feedback case is considered in the rest of this discussion.

Due to the presence of the source current, the wave vectors s, δ, and β will be perturbed and have to be written as $s' = s + \Delta s$, $\delta' = \delta + \Delta\delta$, and $\beta' = \beta + \Delta\beta$. Solving for $\Delta\beta$, we get the coupling coefficient

$$\chi_{pq} = \mathrm{Imag}(\Delta\beta) \quad .$$

It should be emphasized that the presence of boundaries and guided modes has a drastic effect on the coupling coefficient (see Numerical Results and Applications).

The above approach is valid for ϵ and η complex, thus both index perturbation and gain perturbation are covered.

GAIN EFFICIENCY COEFFICIENT

If the guide or the cladding is an active medium of gain coefficient g, the effective gain coefficient will then be equal to Cg with $C < 1$. This is because the optical energy is never completely confined to the guide or the cladding. The coefficient C can be determined by taking complex dielectric constants and solving the dispersion relations for β, which is now complex. In the case of low gain, a first-order Taylor expansion gives:

$$C = \epsilon_1^{1/2}(k/\beta)\ \frac{F}{1+F} \tag{3.17}$$

for an active guide and

$$C = \epsilon_2^{1/2} (k/\beta) \frac{F}{1 + F} \tag{3.18}$$

for an active cladding, where

$$F = \frac{\delta}{s} \frac{f + s\, df/ds}{h + \delta\, dh/d\delta} \quad . \tag{3.19}$$

In the case of an active slab or fiber (TE mode) guide, the coefficient can be determined from simple physical reasoning as

$$C = \frac{P_i}{P_o + P_i} \frac{1}{\cos\phi} \quad , \tag{3.20}$$

where P_i and P_o are, respectively, the power inside and outside the guide, and ϕ is the angle between the optical ray and the z-axis. Both equations (3.19) and (3.20) give the same value for C. A number of plots for different cases are given in figure 3.2.

HIGHER-ORDER INTERACTIONS

High-order Bragg coupling can also be used for feedback. In this case the phase-matching condition is:

$$\beta_p + \beta_q = n2\pi/\Lambda \quad , \tag{3.21}$$

where n is an integer. This could be achieved in two different ways.

If the perturbation is not sinusoidal but a periodic function which can be written in a Fourier series form, then the n^{th} component can be used for phase-matched coupling and all the results of this discussion are valid with η replaced by the n^{th} Fourier coefficient.

Even if the perturbation is sinusoidal, higher-order coupling exists. However, in this case the coupling coefficient is proportional to

$$\chi \sim \eta^n \quad . \tag{3.22}$$

NUMERICAL RESULTS AND APPLICATIONS

All four configurations shown in figure 3.1 were studied in detail. In the case of a thin slab, we considered the distributed feedback due to index sinusoidal periodicity in the guide and the substrate, and for all four configurations we considered the case of sinusoidal boundary perturbation. The major characteristics of interest are: (1) the threshold gain curves as a function of operating wavelength for different longitudinal modes, (2) the longitudinal-modes spectrum, and (3) the longitudinal-field distribution. We first discuss the behavior of the gain coefficient and coupling coefficient. We then discuss in detail the thin-film case and finally present in a more condensed way the properties of the other structures with emphasis on practical applications. For simplicity, in the following discussion all the structures are divided into two regions: In the case of figures 3.1(a) and 3.1(b), the central region will be called "guide" and the outside region "cladding." In the case of figure 3.1(c), the lower half space will be called "guide" and the upper region "cladding."

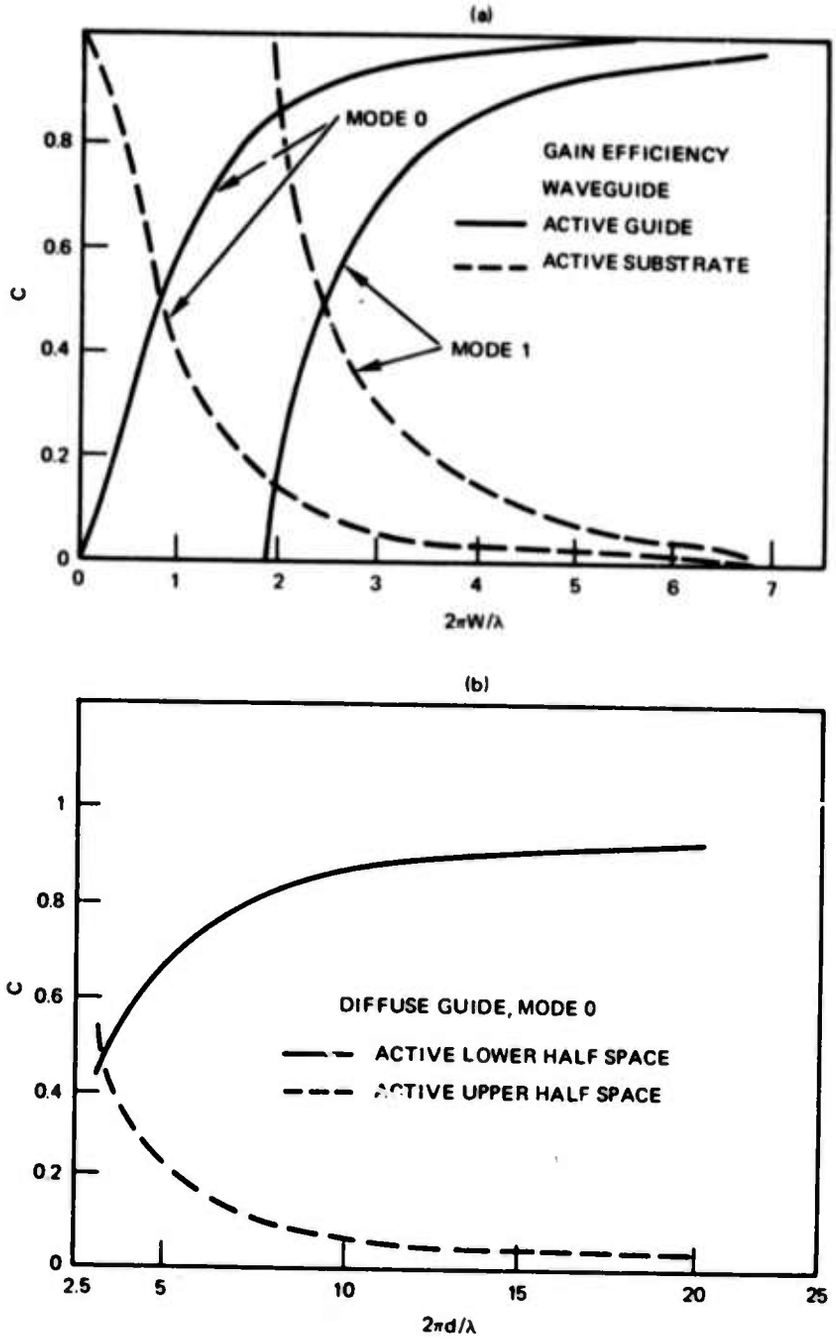

Figure 3.2. Gain efficiency coefficient. (a) Case of a thin film with active guide or substrate. (b) Case of a diffuse guide with active homogeneous or inhomogeneous half space.

In the case of figure 3.1(d), the central region will be called "channel" and the outer region "guide." This notation is so arranged that at high frequency all the energy is in the "guide" region. This is evident in the case of the slab and the fiber. In the case of the inhomogeneous structures the energy tends to concentrate in the high-index region next to the boundary but still in the "guide" region.

GAIN AND COUPLING COEFFICIENTS

The simplest characteristic that could be generalized is the behavior of the gain coefficient C_q. In the case of an active guide, C_q increases from a value $b < 1$ to 1 as the frequency increases away from cut-off, because more energy is concentrated into the guide. Only in the case of the slab and the fiber, $b = 0$. In the case of an active cladding or channel, C_q decreases from b to 0 as the frequency increases. $b' = 1$ for the slab and fiber, and $b' < 1$ in the two other cases. This behavior is clearly seen in figure 3.2.

In the case of a slab with guide index periodicity, the coupling starts at zero near cut-off, because most of the energy is in the substrate, and then increases with the frequency. If the coupled modes are identical, this coefficient levels off when almost all the energy is inside the guide. However, if the coupled modes are not identical, the coupling coefficient reaches a peak and then goes to zero, because the overlap integral vanishes at high frequency (the distributions inside the guide are orthogonal). This behavior is clearly seen in figures 3.3(a) and 3.3(b). This type of periodic structure couples only modes of the same symmetry (even-even or odd-odd).

In the case of a slab with a substrate periodic index, the coupling starts at zero, increases to a maximum, then drops down to zero when most of the energy is confined inside the guide (figs 3.3(a) and 3.3(b).

In the case of surface corrugations, the coupling is small near cut-off because most of the energy is spread in the cladding. At first, the coupling increases with the frequency. In the case of the slab and fiber (fig 3.3) it reaches a maximum then falls off, because the energy concentrates into the guide and the field at the surface becomes very small. In the case of the diffuse guide, the energy tends to concentrate into the high-index region which is next to the perturbed boundary and the coupling continues to increase. At very high frequencies, ηw becomes $> \lambda$, and our theory is no longer valid. This behavior is clearly seen in figure 3.3. A symmetric surface corrugation will couple only even-even modes or odd-odd. An antisymmetric corrugation would couple only even-odd modes. If only one boundary is corrugated, then all types of coupling are possible. In this last case, the value of η has to be doubled in the figures.

SLAB WAVEGUIDE DFB LASER GAIN

In figures 3.4–3.6 we plotted the threshold gain GL required for oscillation and the wave-vector mismatch as a function of the operating wavelength for a number of cases and for different longitudinal modes. Some of these curves show that there are optimum regions where the gain is at a minimum. These regions would correspond to an optimum design. To illustrate, let us consider the case of a surface corrugated DFB laser with gain in the guide and 0-0 mode coupling (fig 3.6(a)). For $\lambda = 0.9\ \mu m$, $2w = 1.2\ \mu m$, $L = 1$ mm, and $\eta = 1.5 \times 10^{-2}$, the threshold gain coefficients for the first three longitudinal modes are, respectively:

$$G_1 = 20\ cm^{-1}\ ,$$

$$G_2 = 27\ cm^{-1}\ ,$$

and

$$G_3 = 30\ cm^{-1}\ .$$

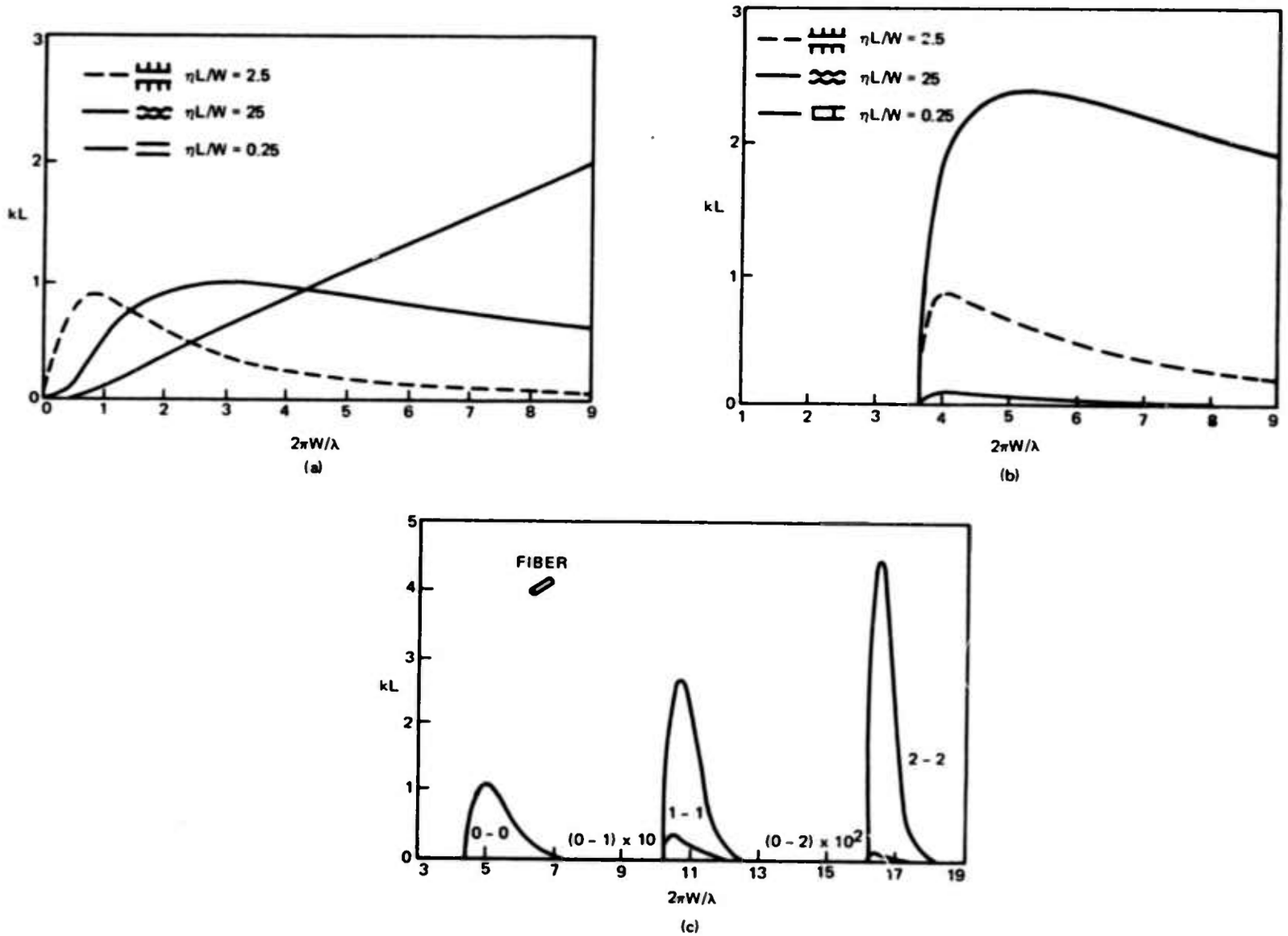

Figure 3.3. Coupling coefficient. (a) 0–0 mode coupling in a thin-film waveguide. The curve for a periodic guide index (light line) levels off at high values of $2\pi w/\lambda$. (b) Coupling coefficient for the 0–2 mode coupling. (c) Different-modes coupling in a fiber as a function of $\eta L/w$.

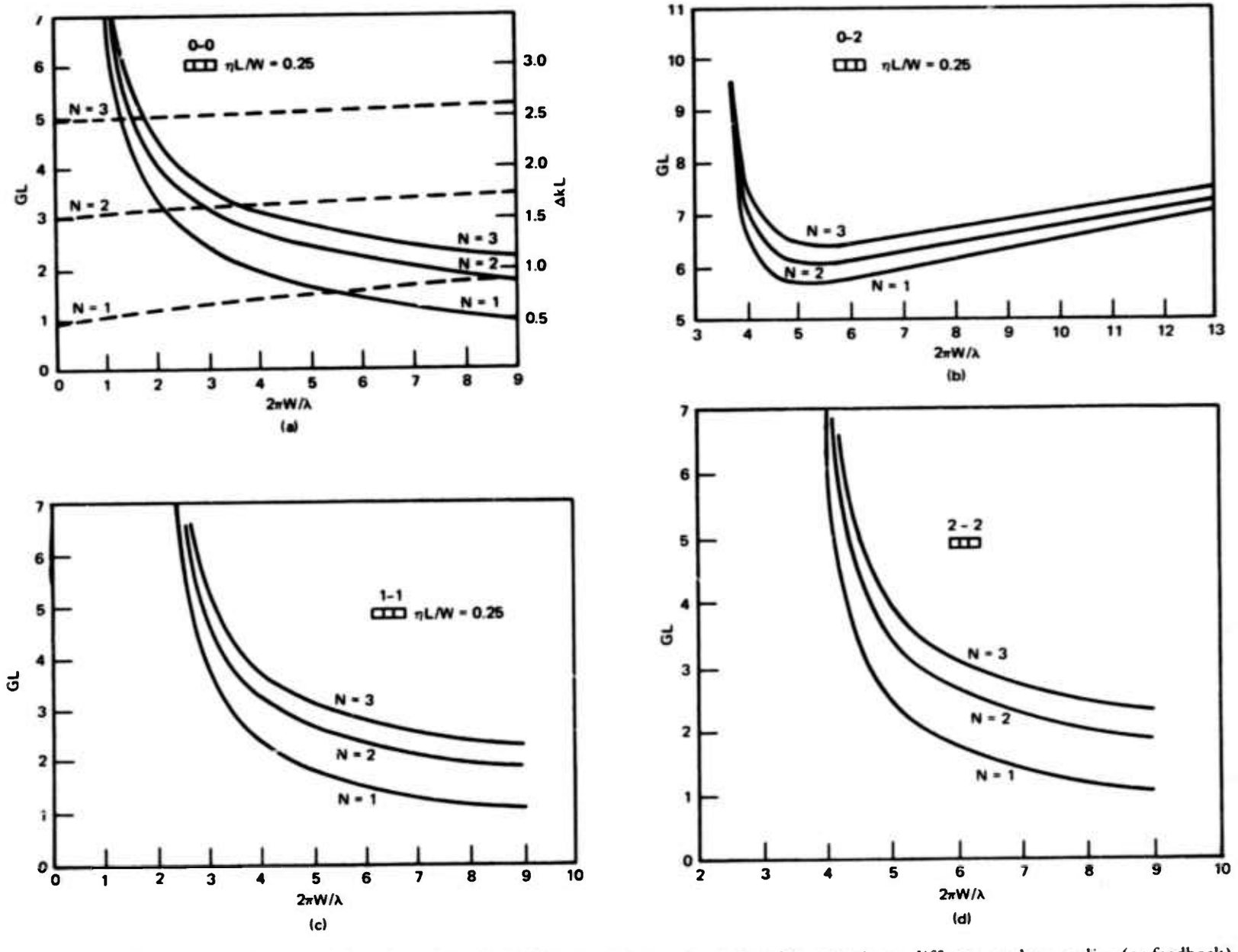

Figure 3.4. Threshold gain coefficient for a thin-film DFB laser with periodic guide index operating at different-modes coupling (or feedback). The dashed lines correspond to the oscillation spectrum (frequency mismatch ΔkL). The different values of N correspond to the different longitudinal spectra.

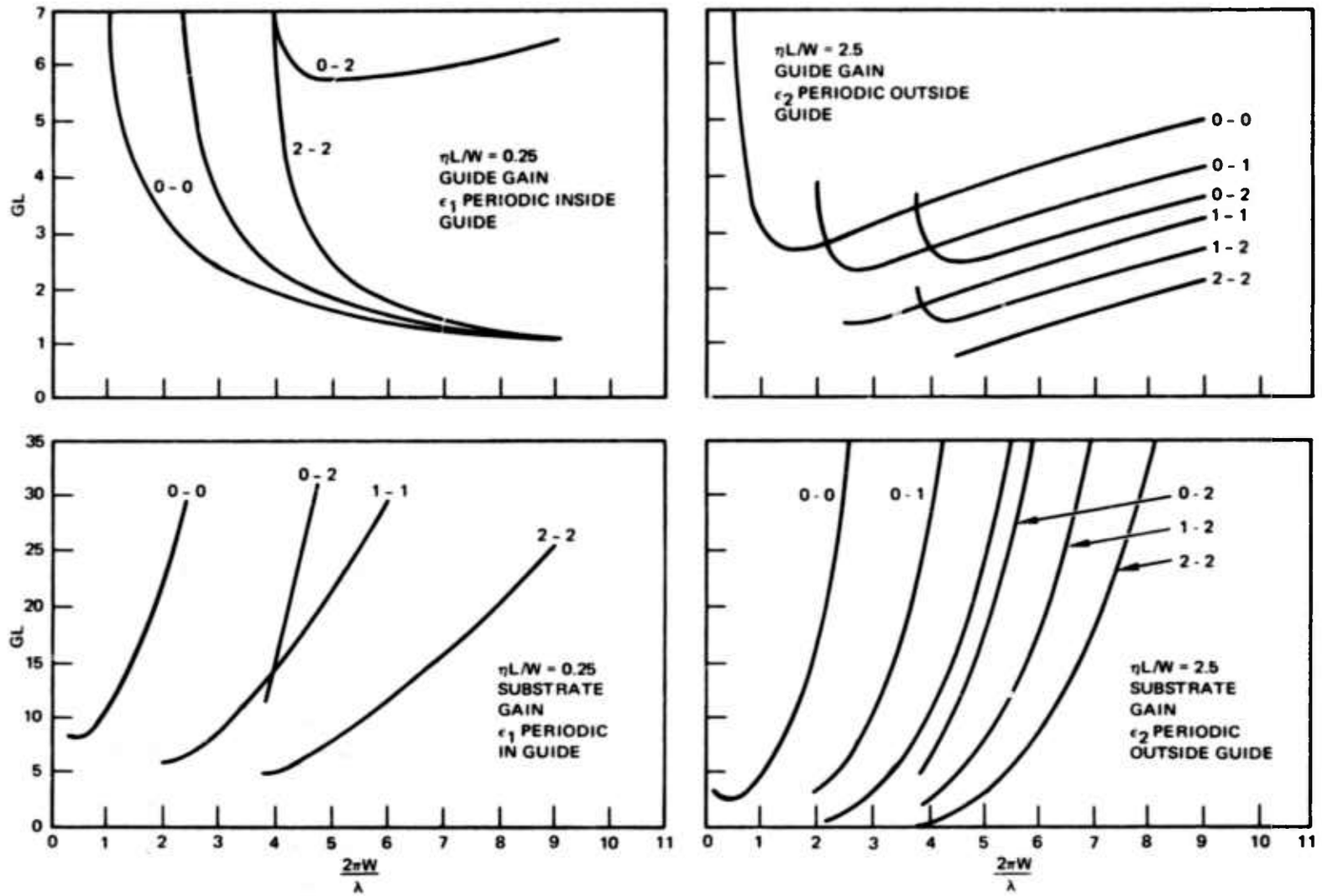

Figure 3.5. Threshold gain coefficient for a thin-film DFB laser with different combinations of: gain in substrate or guide, substrate or guide periodic index, and different-modes feedback coupling.

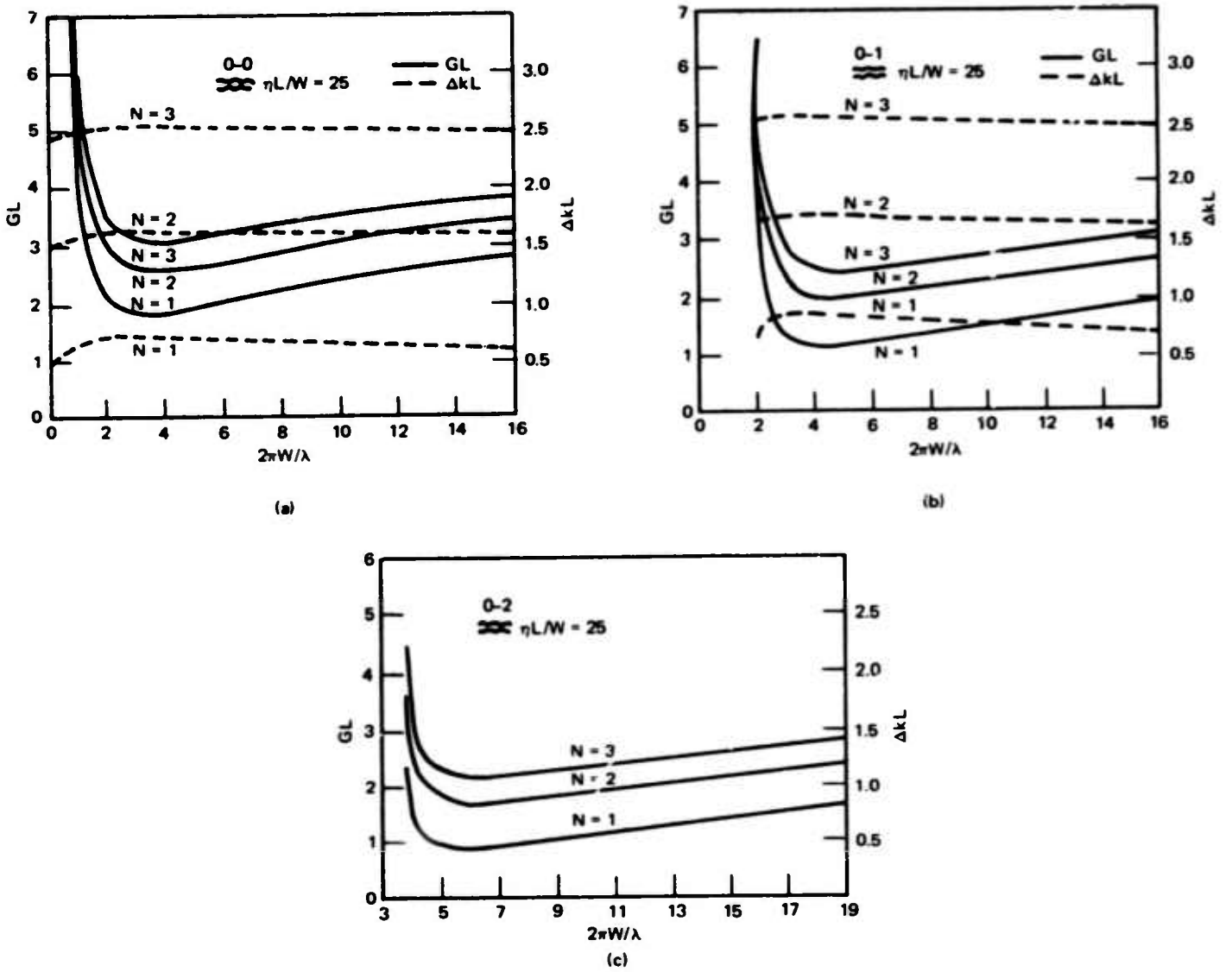

Figure 3.6. Threshold gain coefficient for a thin-film DFB laser with periodic guide boundary operating at different-modes coupling (or feedback). The dashed lines correspond to the oscillation spectrum (frequency mismatch ΔkL). The different values of N correspond to the different longitudinal spectra.

If we consider the 0–1 modes coupling (adequately change the grating period), the threshold gain coefficients drop down to

$$G_1 = 12\ \text{cm}^{-1}$$
$$G_2 = 20\ \text{cm}^{-1}$$

and

$$G_3 = 25\ \text{cm}^{-1} \quad .$$

For the 0–2 modes coupling, the threshold gains are even lower. These gains are well within the limit of available active materials (semiconductors, dye).

It is clear from the curves in figures 3.4–3.6 that the selection of the DFB laser parameter is critical.

In figure 3.7 we plotted the longitudinal intensity distribution in the case of 0–0 and 0–1 coupling in a surface corrugated guide at different frequencies. We remark that the intensity varies appreciably as a function of z, suggesting the fact that, in the case of relatively high-power lasers, where saturation plays a role, the field distribution has to be accounted for in the original coupled equations leading to a nonlinear system of equations.

FIBER DFB LASER

The configuration for a fiber DFB laser that we considered is the one shown in figure 3.1(d). The upper configuration can be achieved by particle beam machining or other techniques. For angularly symmetric TE modes, this configuration is equivalent to the lower configuration, which has a groove depth equal to

$$\eta w = \frac{d}{\pi}\left(\frac{d}{2w}\right)^{1/2} \quad ,$$

which can be derived by Fourier series expansion.

In figures 3.8 and 3.9 we plotted the threshold gain and field distribution for a fiber DFB laser. The general behavior is similar to the case of a slab. To illustrate, let us consider the case where $d/2w = 0.01$, $\eta = 610^{-4}$, $L/w = 6600$, and $\lambda/w = 1.2$. For $\lambda = 1\ \mu m$, this corresponds to $w = 0.83\ \mu m$, $d = 0.016\ \mu m$, and $L = 5.5$ mm. The corresponding threshold gain for the 0–0 mode coupling is (fig 3.8(a)):

$$GL \simeq 3 \Rightarrow \text{total gain} = 25\ \text{dB}$$

for the first longitudinal mode. This gain can be achieved with many active materials (for instance, dye or neodymium doping). A larger value of $d/2w$ would lead to even lower threshold gain.

Such a laser could be used as the light source in an optical network system, thus diminishing the need of coupling from a planar source to a circular guide.

DIFFUSE AND CHANNEL DFB LASER

In figure 3.9 we plotted the threshold gain for the diffuse guide and channel guide for a number of cases. The diffuse guide is attractive because it is very simple to implement. The channel guide can be used in capillary gas lasers with the advantage that the cladding inhomogeneity allows waveguiding. However, it has the disadvantage that the active medium interacts with the evanescent wave only.

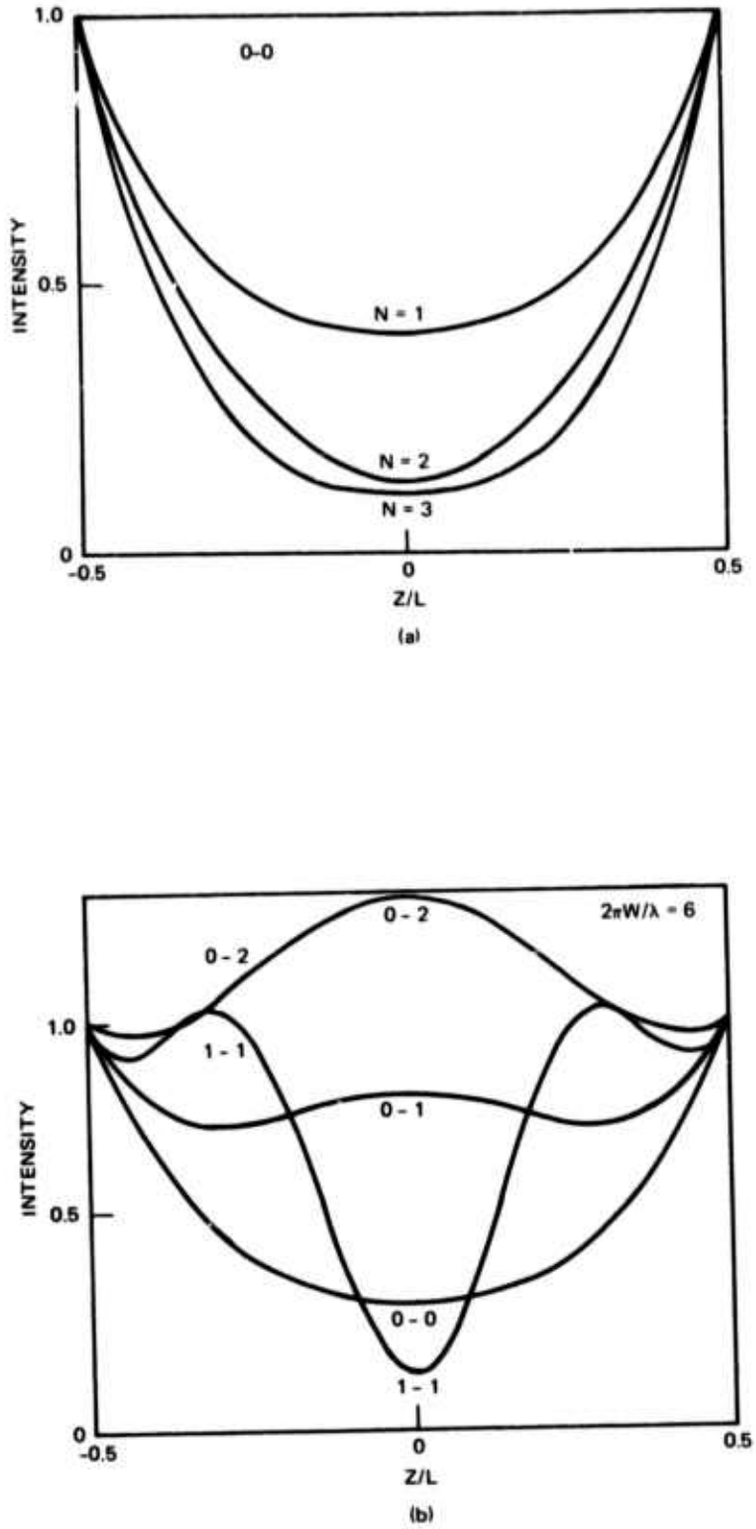

Figure 3.7. Field distribution along a thin-film DFB laser with surface corrugations. (a) Distribution for different longitudinal spectra for 0-0 mode coupling. (b) Distribution for the first longitudinal spectrum but for different-modes feedback coupling.

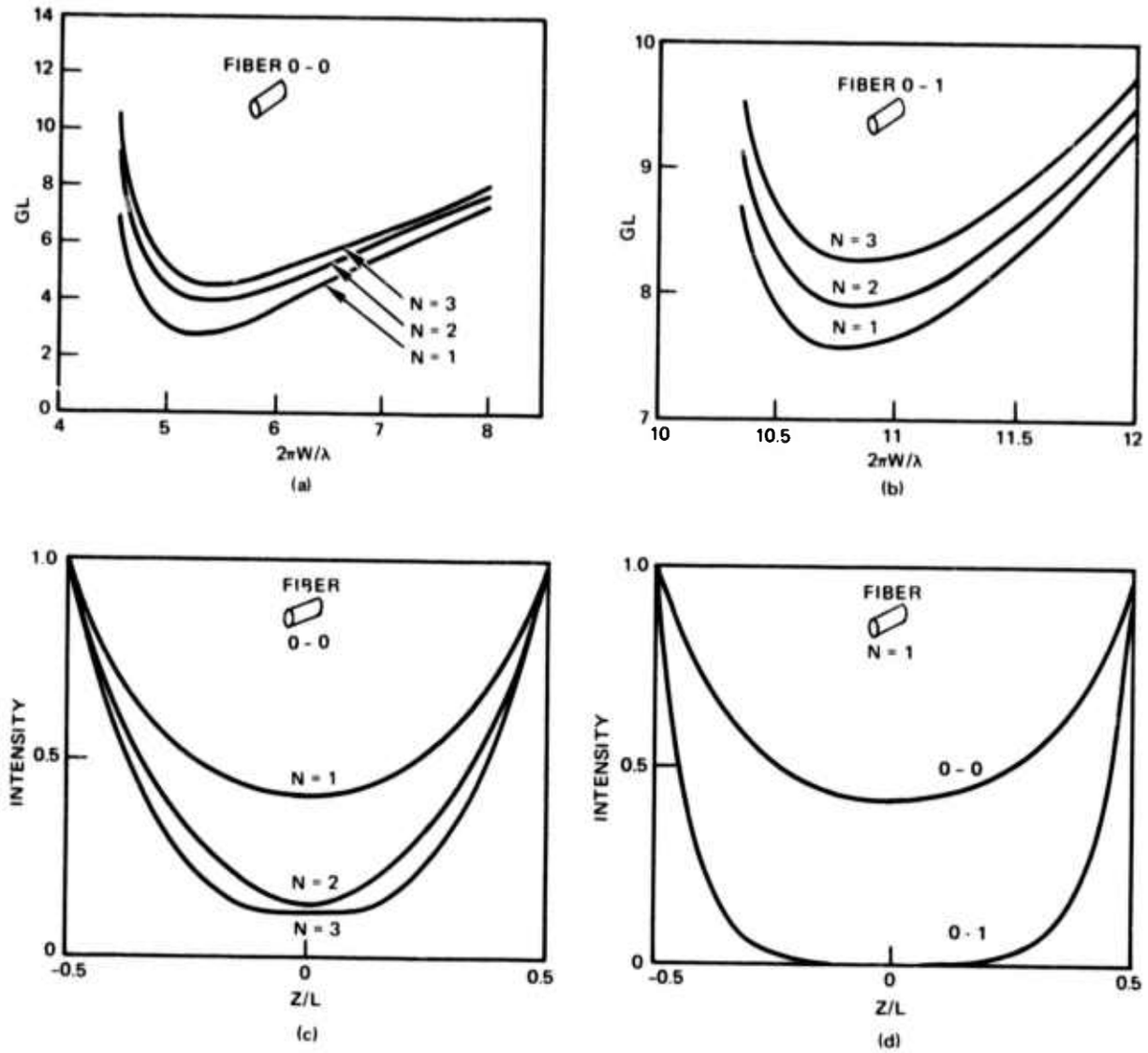

Figure 3.8. Threshold gain coefficient ((a) and (b)) and longitudinal field distribution ((c) and (d)) for a DFB fiber laser.

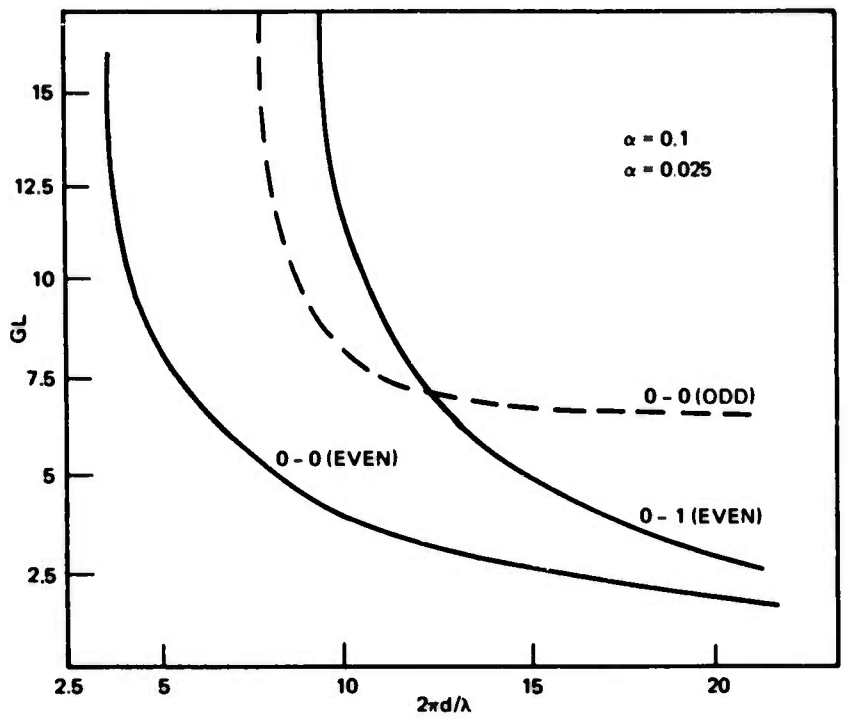

Figure 3.9. Theshold gain for a diffuse capillary DFB laser for different-modes coupling and different values of x.

4. LINEAR WAVEGUIDE AND HORN-SHAPED COUPLING STRUCTURES

Efficient transfer of energy from integrated optical circuits to fiber transmission lines can be achieved by employing special transition fibers to provide the necessary geometric and optical properties for efficient coupling between the structures. Figure 4.1 illustrates the coupling concept. A series of transition fibers that couple external fiber lines to individual waveguides in an integrated optical circuit (IOC) is shown. Interwaveguide switches and/or modulators are contained within the IOC. For purposes of optimizing bandwidth and power consumption properties, the waveguides are as thin and narrow as possible and may be expected to be fabricated of high-refractive-index materials.

A transition fiber is mounted to each output waveguide. The mounting, which may be accomplished for all the waveguides in a single step, is performed under controlled conditions and may be considered a part of the fabrication of the overall integrated optical circuit. The other end of the transition fiber is connected to an external fiber transmission line. This connection process must be capable of being accomplished in the field. By physically separating the transition fibers at the transmission fiber end, coupling adjustment jigs may be used to aid in affixing the fibers. The use of end coupling to optically connect the fibers appears to be the most attractive coupling method from the point of view of minimal processing of the transmission fiber. To accomplish end coupling with high efficiency, the geometric and refractive index properties of the fiber ends must be matched.

With the method of coupling between the transition and transmission fibers established, there remain two conceptual problems. One concerns coupling between the integrated optical waveguide and the transition fiber and the other concerns a method for providing a circular output geometry compatible with the transmission line. Because of geometric and refractive index mismatches, distributed coupling schemes appear the most useful method for achieving waveguide to transition fiber coupling. Distributed coupling can be obtained by fabricating the transition fiber as an externally mounted waveguide of rectangular cross section in the manner indicated in figure 4.2. The coupling itself is obtained by placing a periodic or other layer on the transition fiber and clamping the transition fiber to the waveguide as indicated in figure 4.3.

The externally mounted fiber in figure 4.2 has a rectangular cross section at one end. The cross section gradually changes to circular at the other end. The figure is intended to be symbolic, since such a cross-sectional change would be difficult to fabricate. Geometric conversion to a circular output can be achieved in waveguides wide enough to be multimode with the use of lensing or, to some extent, with shaping methods employing material deposition. An alternative technique for providing a circular output is to use a second transition fiber of circular cross section that is optically coupled to the rectangular fiber. Both fibers may be drawn on the same support fiber or they may be drawn separately and clamped together. The addition of a second transition fiber can only be justified if the insertion loss of the coupling region is low and if mounting a single circular or nearly-circular transition fiber of small diameter to a waveguide is found to be excessively difficult. It is expected that the transition fibers will exhibit low-scattering-loss properties and that high efficiency can be obtained with distributed couplers.

TRANSITION FIBERS

Externally supported glass structures have been investigated as transition fibers. These fibers consist of a rectangular glass section drawn on top of a larger rectangular support fiber which is of lower refractive index. In this configuration the supported fiber is

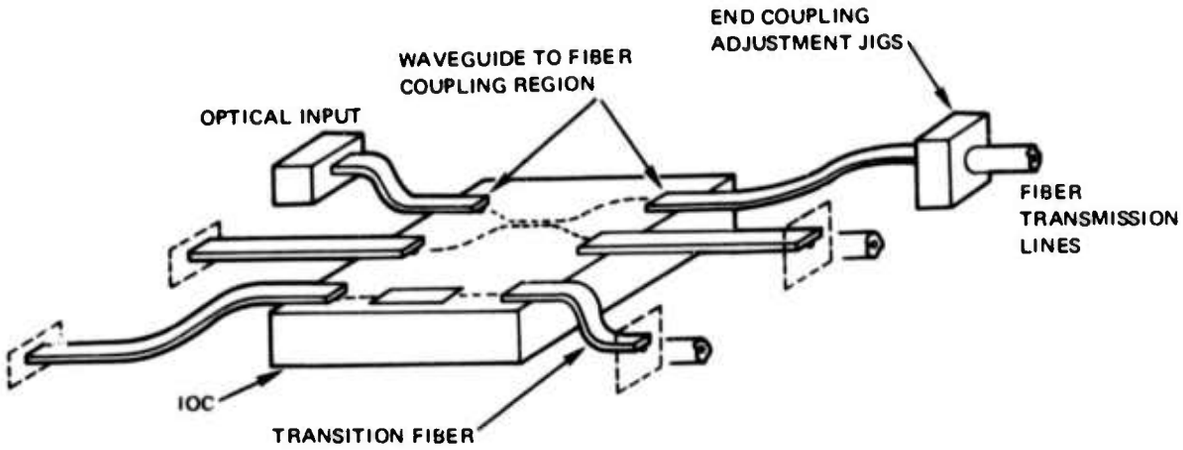

Figure 4.1. Use of transition fibers in optical communications systems.

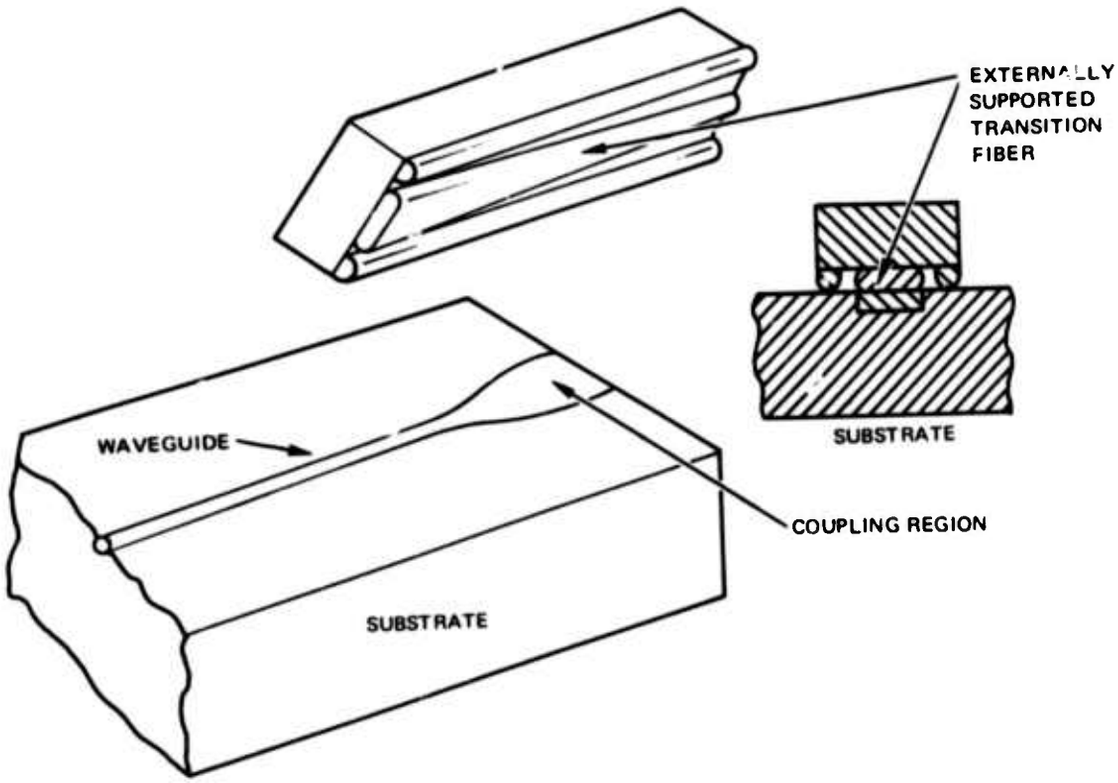

Figure 4.2. Transition fiber to integrated optical waveguide interconnect geometry.

capable of guiding optical waves. It has the major advantage over cylindrically clad fibers that on the unsupported side the guided fields can be readily accessed to allow a variety of distributed coupling techniques to be employed.

Preliminary structures of this type have been fabricated by hand-drawing to a length of several feet. Typical structures consist of a 17 by 6 μm fiber on a 350 by 70 μm support fiber. These were produced by a two-stage process: a 3 by 1 mm scribed portion of a Corning 7059 borosilicate glass microscope slide of refractive index $n_D = 1.53$ was first drawn down to approximately 250 μm by 90 μm; a small length of this fiber was then placed on a 5 by 1 mm scribed Corning 2947 soda lime slide ($n_D = 1.51$) and the composite structure drawn down. A propane flame was used for heating. In the second drawing process, the flame was applied to the back of the substrate in order to prevent distortion of the guiding fiber prior to softening of the substrate. Cross-sectional views of mirror-like fractures of the fibers indicate that a rectangular shape is maintained in the guide with slight rounding of the upper edges.

Guided modes have been launched in the externally mounted fibers by end launching using a focused 633-nm He-Ne laser beam. To obviate the requirement for a polished perpendicular end to the fiber in order to obtain high input coupling efficiency, the fiber end was contacted to a vertical glass slide by means of an index-matching oil (fig 4.4).

DESIGN OF DISTRIBUTED COUPLING STRUCTURES

Two aspects of the design of distributed coupling structures have been studied; the first concerns minimizing the effect of uncertainties and variations in parameter values on coupler performance, and the second concerns optimizing the parameters when their values can be accurately controlled. Achieving an effective coupler in a minimum length is an example of the design objective.

For the case of coupling between two modes, there is one coupler design which is useful in reducing the tolerance requirements on the propagation constants. This model has the propagation constants, k(z), varying linearly in z but in opposite sense for the two guides. A constant coupling coefficient is assumed. At some z the two k(z) will be equal and phase match will occur over a limited region. When the actual values for k(z) differ from the design values for the coupler, phase match will still occur, but the location of this region will be changed.

This model is amenable to analytic solutions, for the resulting second-order differential equations for the mode amplitudes take on the form of classical equations for parabolic cylinder functions.

The analytic solutions to this coupling problem were examined to evaluate the effect of coupling coefficient and rate of change in k(z) on the coupling efficiency and necessary length of the coupler.

The functional rate of change in k(z) can be described by a parameter which is introduced by writing for the two modes:

$$k_1(z) = k_0(1 + \lambda z),\ k_2(z) = k_0(1 - \lambda z) \ . \qquad (4.1)$$

Significant phase match occurs near $z = 0$, and over a distance inversely proportional to λ. A constant coupling coefficient C is assumed, $|C| << k$. The resulting solution can be expressed formally in terms of parabolic cylinder functions of noninteger complex order and of complex argument. No tables exist for these forms, but power series expansions and asymptotic forms are available if numerical results are needed.

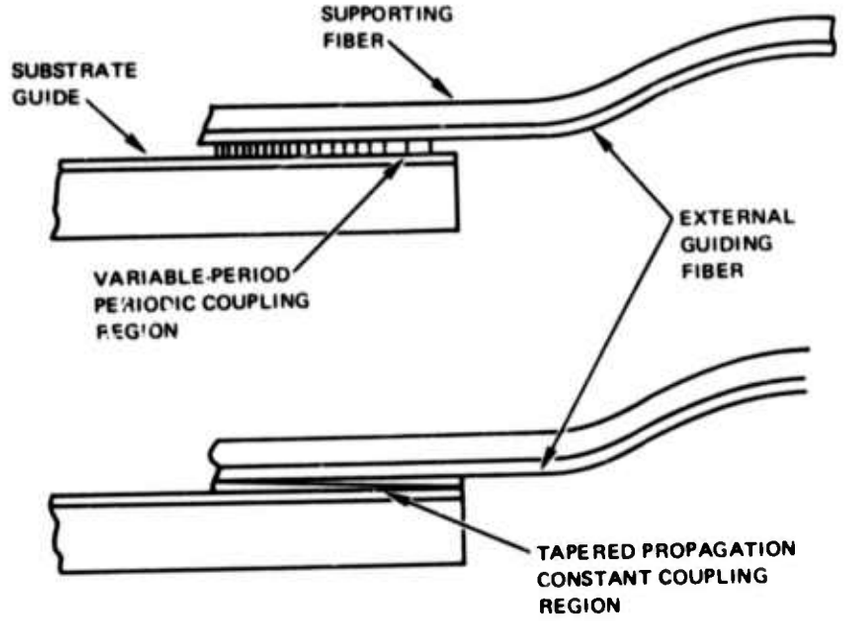

Figure 4.3. Variable-period periodic coupling as a distributed coupling scheme.

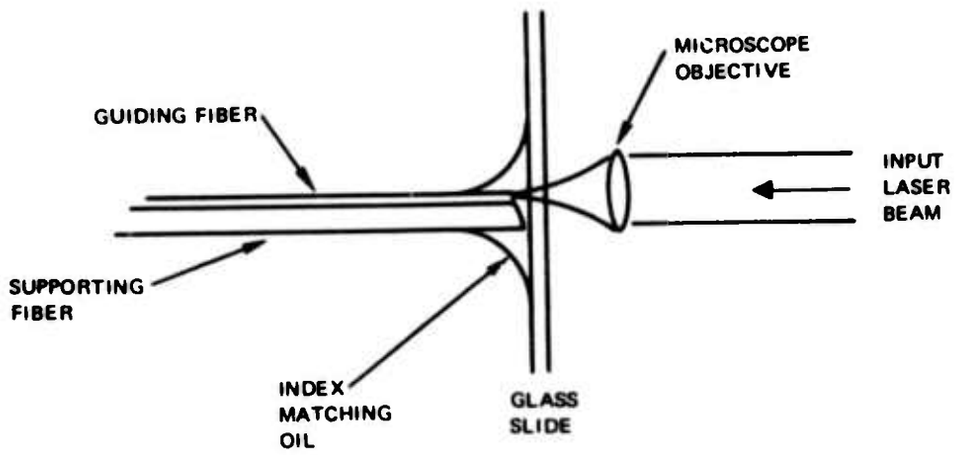

Figure 4.4. Arrangement used to launch waves on an externally mounted fiber.

The solutions are found to depend on C and λ only through a dimensionless parameter, ν, which can be defined as:

$$\nu \equiv C^2/2\gamma k_o \equiv \frac{1}{2}(C/k_o)^2 \cdot (k_o/\gamma) \ . \tag{4.2}$$

The independent argument for the solutions is z times a scale factor which depends only on γ. This dimensionless argument can be written as

$$x \equiv (2\gamma k_o)^{1/2} \cdot z \ , \tag{4.3}$$

so $(2\gamma k_o)^{-1/2}$ is a scale parameter (in the same units as z). This parameter sets the scale, in z, over which power exchanges between modes, and will determine the necessary length of couplers (in contrast to synchronous couplers whose length depends, critically, on C only).

Beyond the region of phase match there is little coupling between modes, and the power in each is constant. In this region asymptotic formulae (power series in $1/x^2$) are available to describe the mode amplitudes; the condition for validity for these is:

$$x^2 \equiv 2\gamma k_o z^2 >> |\nu^2 + \frac{1}{4}| > 1 \ . \tag{4.4}$$

For the case of all the power initially in one mode (say, $P_1[-\infty] = 1$, $P_2[-\infty] = 0$), then the zero-order asymptotic forms for +z, neglecting terms in $1/x^2$, are

$$P_1 \simeq e^{-2\pi\nu} + \frac{2e^{-\pi\nu}\sqrt{1-e^{-2\pi\nu}}}{x} \sin(x^2/2)$$

and

$$P_2 \simeq (1-e^{-2\pi\nu}) - \frac{2e^{-\pi\nu}\sqrt{1-e^{-2\pi\nu}}}{x} \sin(x^2/2) \ . \tag{4.5}$$

Thus, the net power coupled between modes depends exponentially on ν and there is an oscillatory exchange of power which decays as $1/x$. Beyond, say, $x = 10$, the power in each mode will be constant.

With these results it is now possible to say, for example, that if C and γ are such that $\nu = 0.11$, then the power will be equally divided between modes. Also, a 95% efficiency in coupling to the second mode will occur for $\nu = 0.5$, which requires $(\gamma/k_o) = (C/k_o)^2$. The efficiency will not depend on length of the coupler provided it is greater than some value. In general, the length will need to be many (say, up to 10) times the length of a synchronous coupler for the same value of C. These results agree closely with the graph shown by Jones, but the results of Wilson and Teh appear to show considerably higher efficiency for the same parameter values. (The latter described the slope in k by a different choice of parameters, which is somewhat ambiguous).

5. MECHANICAL PROPERTIES OF GLASS FIBER WAVEGUIDES AND FABRICATION OF SPECIAL WAVEGUIDE SHAPES

The fiber pulling machine was approximately completed 1 January and has been in regular use since that time. The maximum length of fiber which can be wound on the drawing drum is 500 meters. The production of longer lengths, if required, will necessitate some modification and installation of a take-up storage reel.

At present the maximum available furnace temperature is 1250°C. This is just enough to permit drawing pyrex-type (borosilicate) glasses.

Feasibility experiments were conducted to make single-mode fibers of silica ($n = 1.4571$) clad with vycor ($n_2 = 1.4562$). Some successful trials were made pulling a rod and tube preformed by hand in an oxyhydrogen torch. Fibers of 100-μm diameter with a 1 – 5-μm core were produced. Previous experience has shown that structures which can be pulled by hand in this way can also be pulled in the fiber drawing machine.

In general, these are exposed guides on supporting substrates, and the shapes attempted to date have been rectangular (for example, 20 by 5 μm) guides or periodic linear structures with about 5-μm spacing. The general approach is to make an appropriate macroscopic structure and then elongate it with the fiber pulling machine while reducing the cross-sectional dimensions.

For example, a 1-mm-thick by 5-mm-wide by 80-mm-long strip of Corning 7059 ($n_D = 1.53$) was placed on a substrate of Corning 7740 ($n_D = 1.47$) which was 6 mm thick by 20 mm wide and the same length. The two pieces were heated to 1200°C and pulled together to elongate the central section by a factor of 4×10^4. The result was a waveguide of dimensions 5 by 25-μm on a substrate of dimensions 25 by 100-μm. More than 50 meters of this structure were produced in a single pull. A view of a fractured end of this waveguide is shown in figure 5.1. A waveguide 10 by 100-μm was pulled in a similar way and is shown in figure 5.2.

A preform for a periodic linear structure was made by placing a row of saw cuts part way through a thick substrate. The saw blade made a 0.25-mm-wide cut, and two cuts per mm produced a regular array with 0.25-mm period. The channels shown in figure 5.3 are about 1 μm wide and the glass spacers are about 6 μm wide. The reduction in cross section expected from the drawing should have produced evenly spaced channels and spacers which were 2.8 μm wide. It is apparent from figure 5.3 that the glass has tended to decrease its height and spread into the channels as a result of flow under surface tension forces during pulling. With suitable adjustments to the relative sizes of the saw cuts and spacers in the preform, a structure with a uniform period of less than 5 μm could be produced.

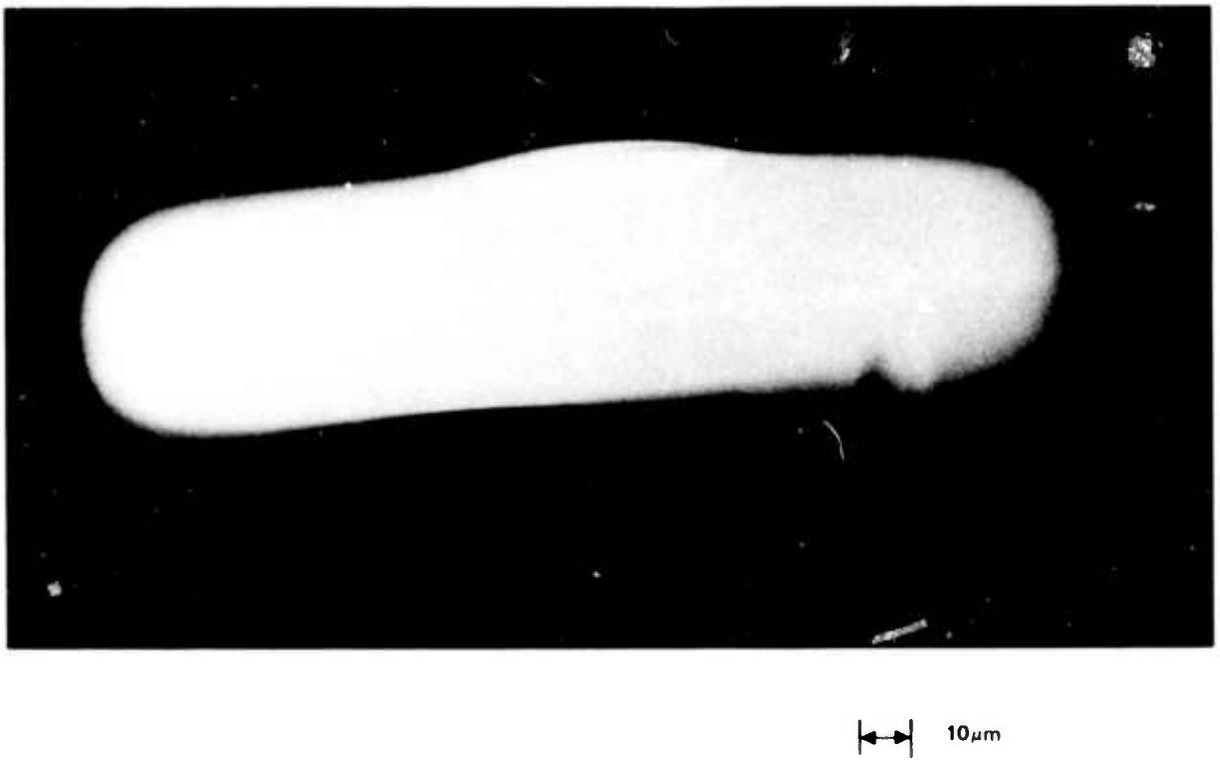

Figure 5.1. Cross section of externally mounted 5-by-25-μm rectangular waveguide (1300X).

Figure 5.2. Cross section of externally mounted 10-by-100-μm rectangular waveguide (1300X).

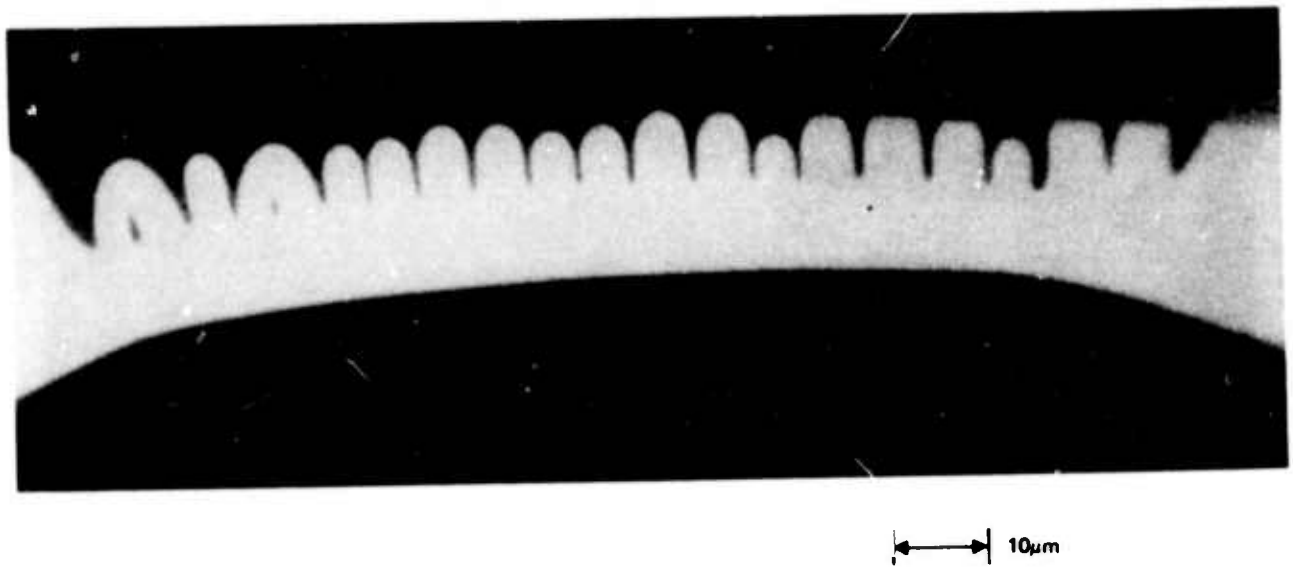

Figure 5.3. Cross section of the drawn structure from a glass slide with row of saw cuts (1300X).

6. POWER REQUIREMENTS FOR FABRICATION OF OPTICAL WAVEGUIDES BY CW LASER HEATING

Practical application of integrated optics devices depends to a large extent on the development of convenient methods for producing single-mode channel waveguides which confine a beam in two dimensions.

A major problem in the fabrication of channel waveguides lies in the size of the groove and in its dimensional tolerance. The width of a single-mode waveguide must be of the order of λ, and wall roughness must be less than a tenth of λ to minimize losses. A new technique has been developed for fabricating very narrow channel optical waveguides. These waveguides overcome this problem. This method allows fabrication of waveguide structures in both passive and electrooptic dielectric substrates.

Originally, the grooves produced by the cw laser beam were filled with a liquid which had a higher index of refraction than that of the filter glass. Waveguiding was observed in the grooves. However, these experiments were discontinued after strong waveguiding was observed under the grooves without any filling.

WAVEGUIDE FABRICATION

The apparatus for fabricating the waveguides is illustrated in figure 6.1. The 488-nm line of a Spectra Physics Model 164 argon ion cw laser is focused with a 20-power Bausch and Lomb microscopic objective on the surface of a 1-mm-thick glass filter. In most of the experiments, a 2 by 1/4-inch piece of OG 550 JENA color filter was used. The color filter glass was obtained from Fish-Schurmax Corp. Probably, OG 530 could also have been used. Grooves were also produced on OB 570, OG 590, RG 610, and RG 630. However, the RG 630 started to absorb the 632.8-nm line of the He-Ne cw laser which was employed for the waveguiding experiments. All these filters strongly absorb the 488-nm line.

The color filter was mounted on an assembly which consisted of three translation stages to provide precision motion in the X, Y, and Z directions. The X and Y stages allowed movement perpendicular to the focused laser beam. The Z direction was used for focusing.

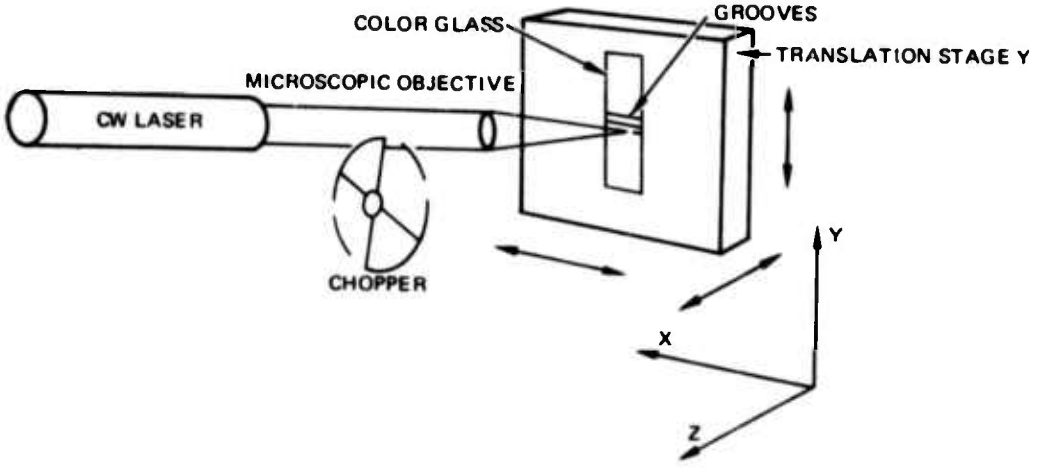

Figure 6.1. Experimental arrangement. The sample is mounted on an assembly consisting of three translation stages for movement in the X, Y, and Z directions. Only the Y-direction translation stage is shown. As this stage is moved up or down, arrays of parallel grooves are produced on the sample.

Straight grooves were produced by moving the colored glass at constant speed in the X direction. This was accomplished by connecting the differential screw of the X stage to a variable-speed electric motor with the aid of a flexible cable. One motor could be varied in speed between 0 and 17 r/min, resulting in a sample speed from 0 to 270 μm/sec. The other motor operated between 0 and 96 r/min, which corresponded to a sample speed from 0 to 1700 μm/sec.

The Y translation stage was a precision stage obtained from Lansing. It allowed moving the color filter up or down to fabricate parallel grooves and had an accuracy of 0.13 μm/div. One could also attach an electric motor to this stage as in the Y stage. This would make it possible to fabricate bends and related structures.

Proper focusing of the laser beam on the surface of the sample for writing small grooves presented a major problem. Rough focusing was present when maximum reflection of laser light was observed from the surface of the sample. This area covered a range of about 3 μm. Fine focusing had to be accomplished by trial and error. The smallest grooves produced were about d = 2 μm wide. However, these grooves could be produced only with very close focusing, which was rarely achieved. Often, only the beginning or end of the narrow groove would show up on the sample. In addition, because of the low resolution of conventional microscopes, the width of these grooves could not be measured exactly. The waveguiding properties of the 2-μm-wide grooves were not good. However, grooves wider than 3 μm, possessing very good waveguiding qualities, could consistently be produced.

To observe waveguiding, an experimental setup was employed consisting of a 1.5-mW He-Ne cw laser, two microscopic objectives mounted as translation stages for input/output coupling, and an observation microscope. One microscopic objective coupled the laser light into the guide in an end-fire configuration and the second projected the near-field pattern of the end of the waveguide onto a white screen.

Finally, waveguides with corrugations (periodically varying thickness) can be fabricated by the partial insertion into the laser beam of a mechanical chopper.

WAVEGUIDING OF A SINGLE GROOVE

Figure 6.2 presents a photograph of a side view of a groove about 4 μm wide, produced by about 320-mW power at a sample speed of 0.5 mm/sec (fig 6.2(a)). The pattern of the guided helium-neon cw laser beam (633 nm) is shown in figure 6.2(b).

When the guiding groove is viewed from the top with the aid of a microscope, no scattered light line is observable. This indicates that scattering losses are low. The low-loss property of these grooves – indicating smooth edges – is not surprising, because of their thermal origin.

Figure 6.3 shows a photograph of the end view of some grooves. Several interesting observations can be made: (1) The grooves have no surface ridges, suggesting that material has disappeared. This leads to the conclusion that the temperature created at the focal point due to the strong absorption by the glass filter is sufficiently high to evaporate some of the glass. (2) Around the grooves, especially under them, a considerable change in shade is evident. This indicates a change in the index of refraction of the glass in this area. Obviously, the occurrence of optical waveguiding in this region indicates that the index of refraction has increased. Heat generates strain in most glasses, and this strain must lead to the change of refractive index. The type of filter color glass employed in these experiments obtains its color from dissolved metal oxides. The high temperature created at the focal

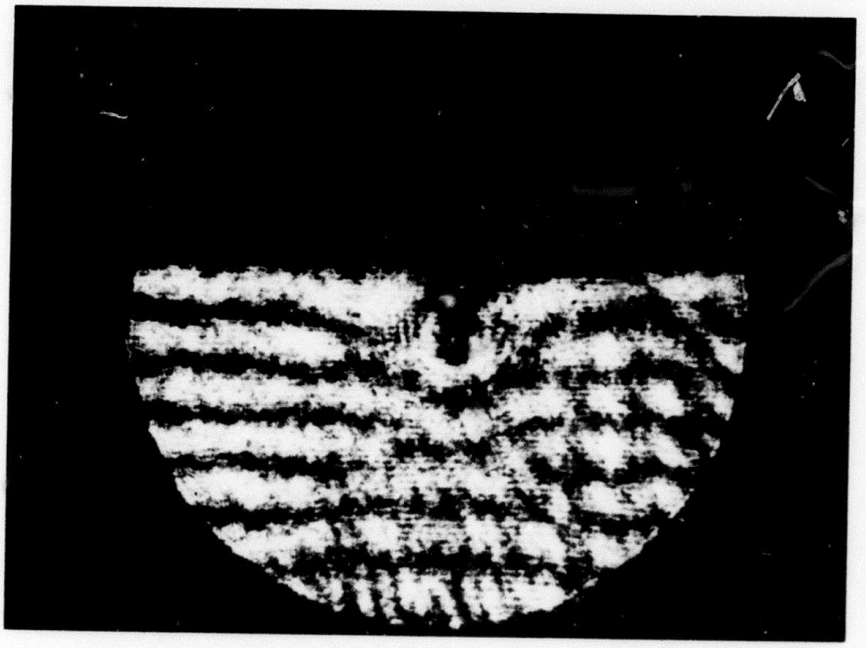

(a)

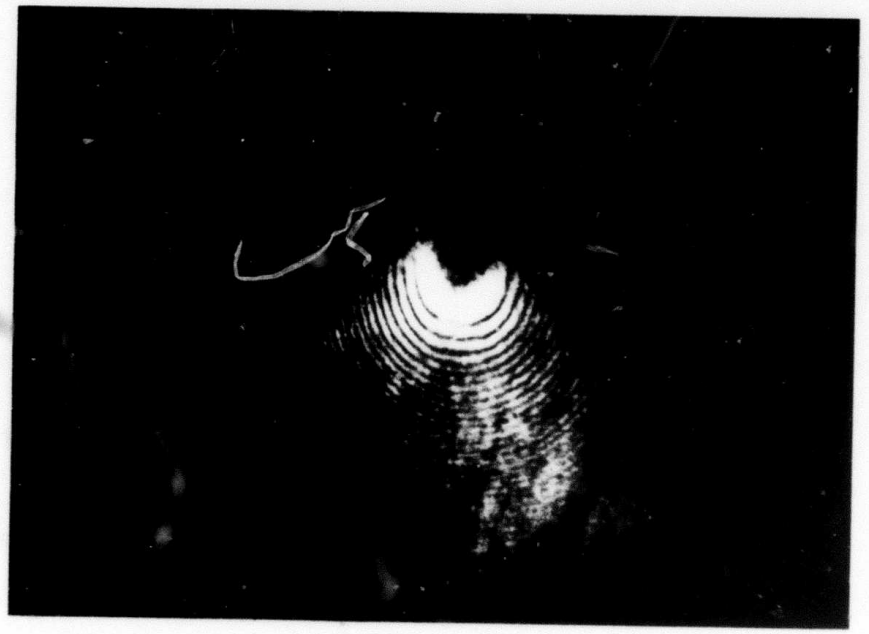

(b)

Figure 6.2. (a) Mispositioned laser input spot showing a Lloyd's mirror interference effect, causing fringes on the inside of the color glass. The grooved area is located in the middle of the picture, shown by the dark contour. (b) Optical waveguiding. The input laser beam is properly positioned and light is confined within a guiding area under the grooves.

Figure 6.3. Photograph of the side view of three grooves taken through a microscope. All grooves were written with the same power (P = 320 mW) but different translation rates v. Left groove was produced at v = 150 μm/sec, and is 6.5 μm wide and about 40 μm deep. Middle groove was produced at v = 630 μm/sec, and is 4.5 μm wide and about 30 μm deep. Right groove was produced at v = 160 μm/sec, and is 3.2 μm wide and about 20 μm deep.

point of the laser might also cause some composition changes in the glass, which could contribute also to the change in refractive index. Finally, the high electric fields present at the laser focal point could also have a polarization effect, which would also cause changes in refractive index. (3) The grooves are rather deep with respect to their width.

PARAMETERS WHICH DETERMINE GROOVE SIZE

To determine the relationships between laser power applied, groove size, speed of sample, and efficiency of waveguiding, several experiments were performed. The results obtained need the additional precision of electron microscopy to measure groove width, d, accurately. The conventional microscope used in the experiments reported here allowed a determination of groove width to ±0.2-μm. Figure 6.4 presents groove width as a function of laser power applied at constant translation speed. The power of the beam was measured with a meter positioned inside the laser. However, the power values shown in figure 6.4 are high. The laser beam, after passing through the spatial filter and the microscopic objective, could have lost about 25% of its original value.

From figure 6.4 it is apparent that the relation between applied power P and d for a certain speed v is a linear one:

$$P = md + P_1 \ . \tag{6.1}$$

At different speeds, one obtains straight lines passing through the same point P_o.

$$P = m(v)d + P_o \ . \tag{6.2}$$

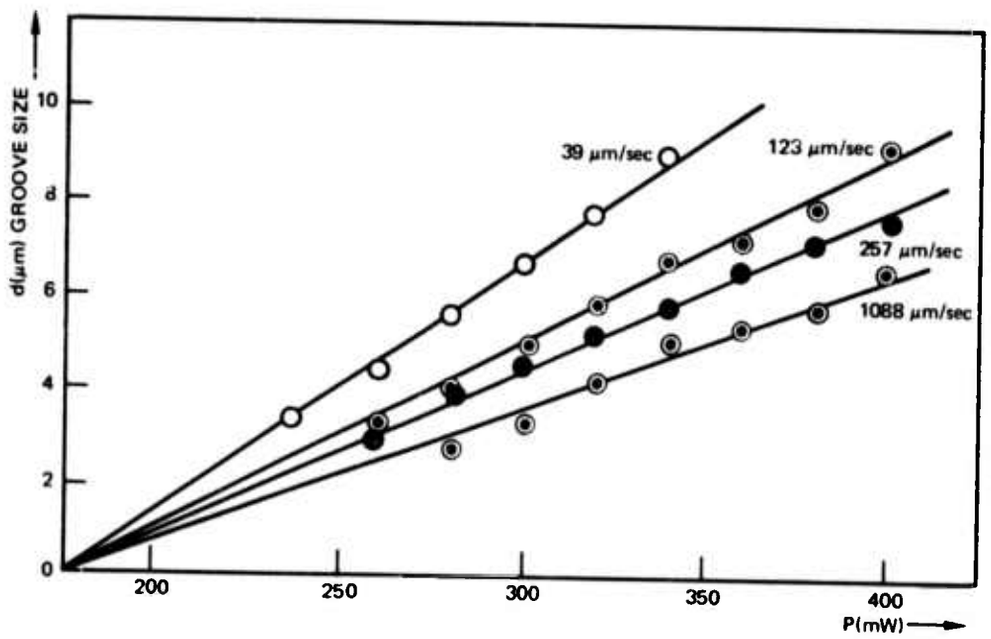

Figure 6.4. Plot of groove size d (μm) as a function of applied power P (mW) at four different translation speeds v (μm/sec).

This simple relation is difficult to understand. It would suggest that the same minimum power P_0 is always required before a groove is produced, independent of translation rate v. Any power applied above P_0 evaporates some of the material producing a groove. P_0 represents power losses due to reflection of the laser light from the surface of the sample plus losses from heat convection. The losses resulting from reflection should be more or less independent of translation speed v. However, power losses from heat convection should be dependent on speed v. Possibly, losses from heat convection are small.

The slope m(v) does not change much, even if the speed is changed over a wide range. This may suggest that the slope m(v) depends logarithmically on the speed v. Figure 6.5 seems to confirm this assumption. Indeed, plotting the speed v on a logarithmic scale as a function of the slope m yields a straight line. Consequently:

$$P = a \log v\, d + P_0 \ . \qquad (6.3(a))$$

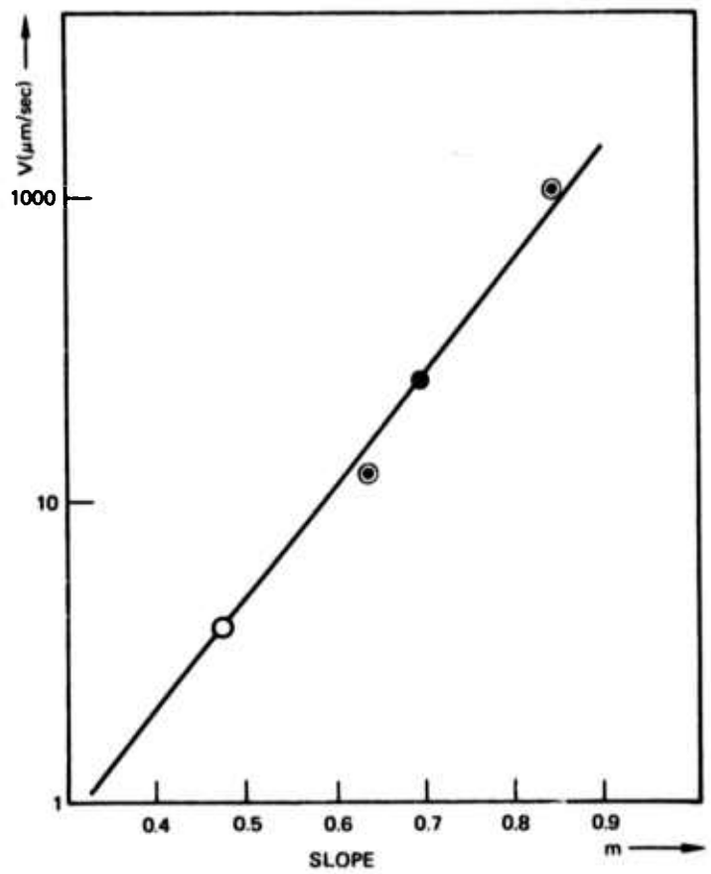

Figure 6.5. Plot of the four different slopes m_1 (⊙), m_2 (○), m_3 (●), and m_4 (◉) as functions of the different translation speeds v.

It was felt that the validity of relation (6.3(a)) should be tested further, because it rests on only four points (slopes m). A large number of grooves were produced at constant power (P = 320 mW) but at many different speeds. P = constant implies:

$$P - P_o = a \log v\, d \qquad (6.3(b))$$

or,

$$d = -M \log v + N \ . \qquad (6.4)$$

This equation is indeed confirmed by the experiments. Groove size plotted as a logarithmic function of speed (fig 6.6) yields a straight line with negative slope.

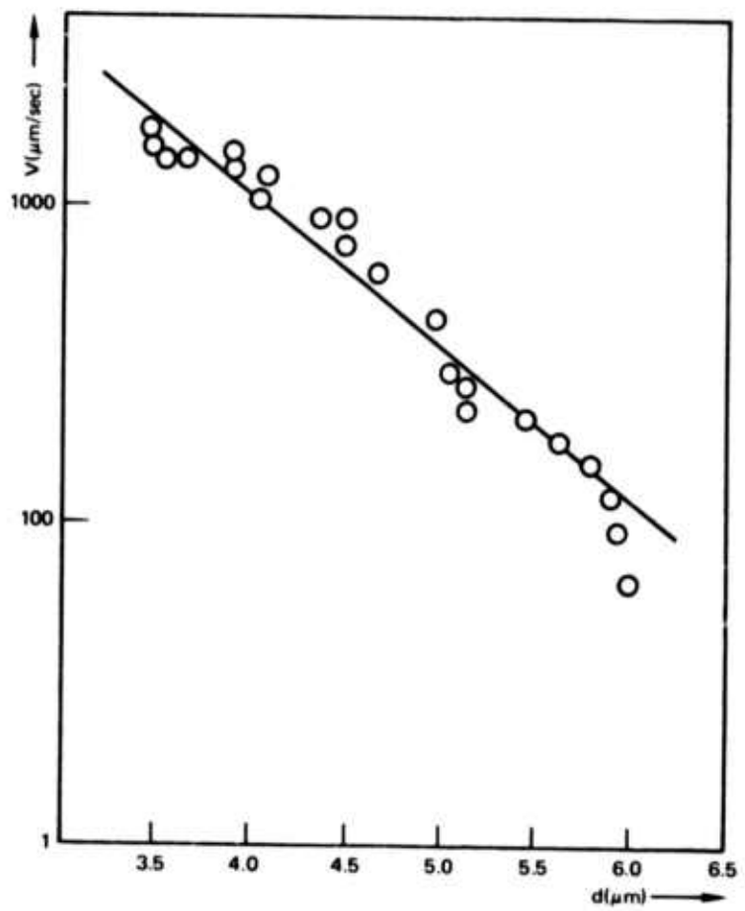

Figure 6.6. Plot of groove size d (μm) as a function of translation speed v (μm/sec). v is presented on a logarithmic scale. All grooves were written with the same power (P = 320 mW).

WAVEGUIDING PROPERTIES

Of more importance than the above relations between cw laser power applied, speed of writing, and groove size, are the waveguiding properties of the grooves. For example, one would like to know how applied power, translation rate, and waveguiding properties are interrelated. To obtain information on some of these questions, several grooves were fabricated at constant power (P = 320 mW) but at different speeds v (translation rates).

Two sets of grooves were fabricated at the same power and translation speeds. To measure the intensity of the guided light (relative power out), the second microscopic objective was adjusted to project the collected light of the chopped laser light on a PIN diode. The relative power out was recorded with the aid of a lock-in amplifier. Maintaining constant input coupling into each of the two different sets was difficult. In order to obtain comparable results, the sample must be moved exactly perpendicularly to the focused laser beam. The amount of relative power out also depends critically on the focusing itself and at what point under the groove the light is focused. Although it was not possible to find the exact alignment which would have produced the same power out for the two different sets of grooves produced, the experimental results presented in figure 6.7 are informative. Good

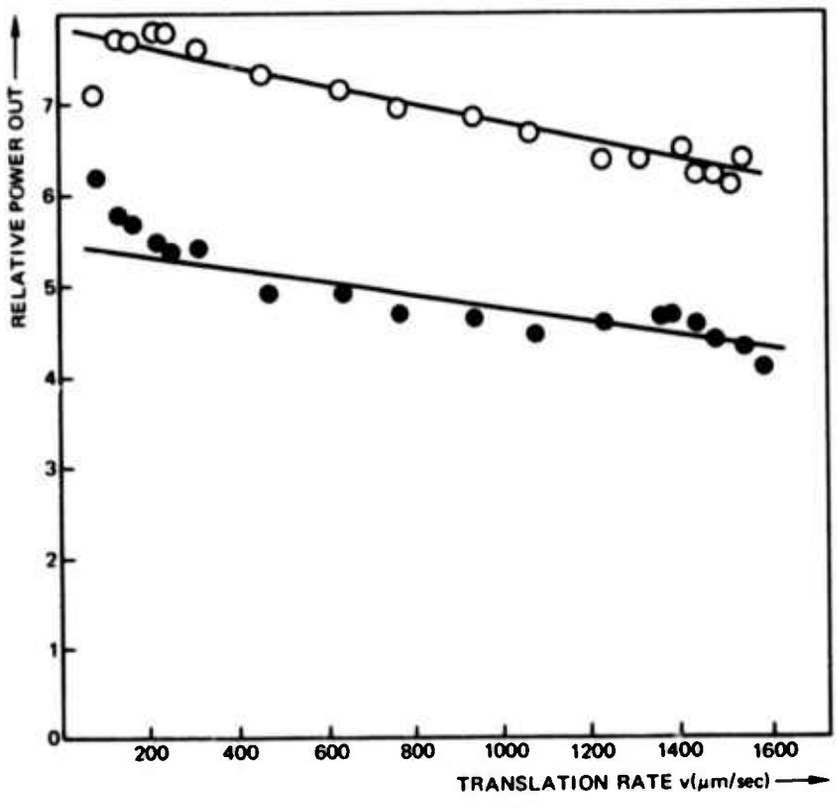

Figure 6.7. Relative power out of optical waveguides (grooves) fabricated at different translation rates v (μm/sec) but the same power (P = 320 mW). The figure shows measurements on two identical sets.

waveguiding seems to be present over an exceptionally wide range of translational speeds (from 100 to 1600 μm/sec). Although this amount of relative power out decreases steadily with increasing speed, this does not necessarily imply that the waveguiding quality of the grooves gets poorer. With increasing speed, the grooves become narrower, which means that the guiding area would also become smaller, resulting in a simpler mode structure of the guided light. However, with smaller guiding area, the difficulty of coupling light efficiently into the waveguides also increases. This may explain the small decline of relative power out with larger speeds. No electric motor was available which could be driven at translation speeds greater than 1600 μm/sec. The highest translation speed employed (1.6 mm/sec) is actually very high. Consequently, grooves with good guiding properties can be fabricated at fast translation rates. This fact should be significant for mass production of channel waveguides and derived structures by the method described in this article.

FREQUENCY-SELECTIVE WAVEGUIDES

Waveguides with periodically varying thickness should be frequency selective in their waveguiding properties. If one employs a chopper having 16 plates which is driven by an electric motor at 3000 r/min, and the sample moves at a translation rate of v = 160 μm/sec, periods as small as 0.2 μm can easily be obtained.

Figure 6.8 shows a photograph, obtained with the aid of a microscope, of a waveguide fabricated at v = 154 μm/sec, cutting off 3/16 inch of the 5/8-inch-wide laser beam. The 16-plate chopper was driven at 49 r/min.

An important problem in integrated optics circuitry is the coupling of guided light from one waveguide into another. One solution to this problem may be to use a center waveguide and two parallel waveguides, the waveguide on the left side of the center waveguide having a period of λ_1/n and the one on the right a period of λ_2/n. If the two waveguides are positioned at the proper distance and have the proper length, frequency-selective coupling between these channel waveguides should take place.

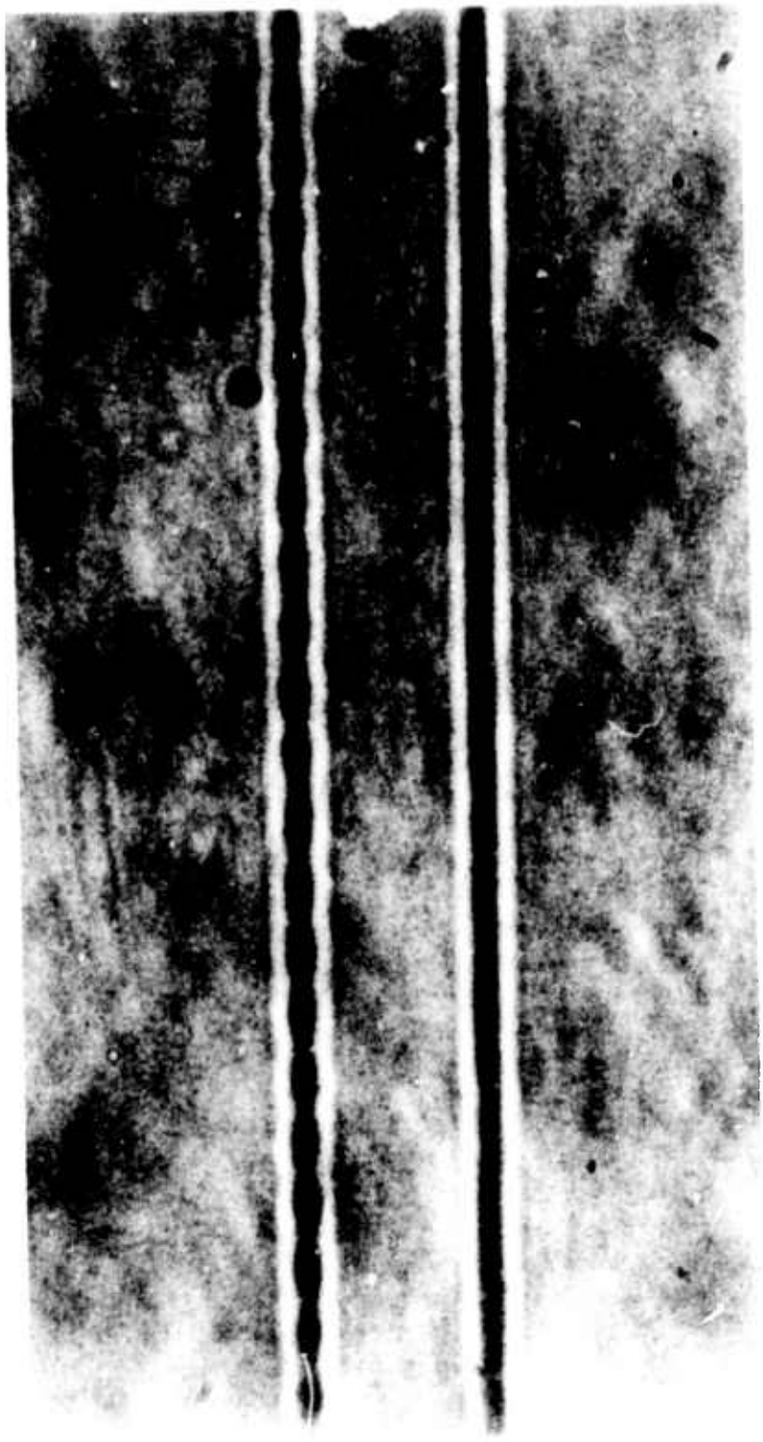

Figure 6.8. Waveguide with periodic structure. The top waveguide was produced without inserting the mechanical chopper. Both grooves were fabricated with a power P = 320 mW and a translation rate v = 160 μm/sec. The top groove is about d = 5 μm wide. The periodic groove is also 5 μm in thickness at its widest part. The period is about 11 μm and was produced with a 16-blade chopper, rotating at about 490 r.p.m.

APPENDIX: INTEGRATED OPTICS REPRINTS, TALKS, AND PUBLICATIONS

1 H. F. Taylor, W. E. Martin, V. N. Smiley, and D. B. Hall, "Fabrication of Optical Circuits by Solid State Diffusion," OSA Topical Meeting on Integrated Optics, Las Vagas, 7 February 1972

2 H. F. Taylor, W. E. Martin, D. B. Hall, and V. N. Smiley, "Fabrication of Single Crystal Semiconductor Waveguides by Solid State Diffusion," Appl. Phys. Lett. 2195, 1972

3 W. E. Martin and D. B. Hall, "Optical Waveguides by Diffusion in II-VI Compounds," Appl. Phys. Lett., 21,325, 1972

4 H. F. Taylor, V. N. Smiley, W. E. Martin, and S. S. Pawks, "Fluorescence of Graded-Band-Gap CdS_xSe_{1-x} Crystals Produced by Diffusion," Phys. Rev. B.5, 1467, 1972

5 D. B. Hall and W. E. Martin, "Diffused Optical Waveguides in II-VI Compounds," Quantum Electronics Conference, Montreal, 1972

6 D. B. Hall and C. Yeh, "Leaky Waves in A Heteropitaxial Film," J. Appl. Phys. 44, 2271, 1973

7 H. F. Taylor, "Optical Switching and Modulation in Parallel Dielectric Waveguides," J. Appl. Phys. 44, 3257, 1973. ONR

8 H. F. Taylor, "Frequency Selective Coupling in Parallel Dielectric Waveguides," Opt. Comm. 8, 421, 1973

9 D. J. Albares, "Military Applications of Fiber and Integrated Optics," NSF Grantee-Users Conf. on Optical Comm., Washington University, St. Louis, 14 November 1973

10 W. E. Martin, "Photoluminescence Determinations of Cd Diffusion in ZnSe," J. Appl. Phys., December 1973

11 W. E. Martin, "Waveguide Electro-Optic Modulation in II-VI Compounds," J. Appl. Phys. 44, 3703, 1973

12 C. Elachi and C. Yeh, "Frequency Selective Coupler for Integrated Optics Systems," Opt. Comm., 7 201, 1973

13 H. F. Taylor, "Fiber Optics Communications," Naval Research Reviews, January 1973

14 W. M. Caton, W. E. Martin, D. B. Hall, H. F. Taylor, "Diffused Waveguides and Modulators in II-VI Compounds," OSA Topical Meeting on Integrated Optics, New Orleans, 21 January 1974

15 C. Elachi, G. Evans, C. Yeh, "Parametric Optimization of Thin-Film DFB Lasers," OSA Topical Meeting on Integrated Optics, New Orleans, 21 January 1974

16 C. M. Stickley, D. J. Albares, H. F. Taylor, T. G. Giallorenzi, A. F. Milton, "Anticipated Uses of Fiber and Integrated Optics in the Defense Department," OSA Topical Meeting on Integrated Optics, New Orleans, 21 January 1974

17 R. K. Winn, J. H. Harris, "Coupling from Planar to Linear Guides Using Horn Shaped Structures," OSA Topical Meeting on Integrated Optics, New Orleans, 21 January 1974

18 H. L. Garvin, E. D. Wolf, "Ion and Electron Beam Fabrication of Optical Components," OSA Topical Meeting on Integrated Optics, New Orleans, 21 January 1974

19 H. F. Taylor, "Optical Modulation in Thin Films," J. Vac. Science and Technology (ONR), v 11, n 1, January/February 1974

20 H. F. Taylor, "Power Loss at Directional Change in Dielectric Waveguides," Applied Optics, v 13, n 3, March 1974

21 D. J. Albares, "Navy Applications of Fiber Optics and Integrated Optics," Integrated Optics and Fiber Optics Communications Conference, Naval Electronics Laboratory Center, San Diego, 15 May 1974

22 C. Yeh, "Optical Waveguides," Integrated Optics and Fiber Optics Communication Conference, Naval Electronics Laboratory Center, San Diego, 15 May 1974

23 J. H. Harris, "Coupling Problems in Optical Communications," Integrated Optics and Fiber Optics Communications Conference, Naval Electronics Laboratory Center, San Diego, 15 May 1974

24 G. A. Chutaramayya and W. D. Scott, "Fabrication of Special Shapes for Optical Waveguides," Integrated Optics and Fiber Optics Communications Conference, Naval Electronics Laboratory Center, San Diego, 15 May 1974

25 W. Caton, E. D. Wolf, "Fabrication of Single Mode Optical Waveguides in II-VI Compounds for Integrated Optical Circuits," Integrated Optics and Fiber Optics Communication Conference, San Diego, 16 May 1974